A&A 450, 777–791 (2006)
DOI: 10.1051/0004-6361:20054223

Astronomy & Astrophysics

Searching for links between magnetic fields and stellar evolution

I. A survey of magnetic fields in open cluster A- and B-type stars with FORS1⋆,⋆⋆

S. Bagnulo[1], J. D. Landstreet[2], E. Mason[1], V. Andretta[3], J. Silaj[2], and G. A. Wade[4]

[1] European Southern Observatory, Casilla 19001, Santiago 19, Chile
e-mail: sbagnulo@eso.org;emason@eso.org
[2] Physics & Astronomy Department, The University of Western Ontario, London, Ontario, N6A 3K7, Canada
e-mail: jlandstr@astro.uwo.ca;jsilaj@uwo.ca
[3] INAF – Osservatorio Astronomico di Capodimonte, salita Moiariello 16, 80131 Napoli, Italy
e-mail: andretta@na.astro.it
[4] Department of Physics, Royal Military College of Canada, PO Box 17000, Station "Forces" Kingston, Ontario, K7K 7B4, Canada
e-mail: Gregg.Wade@rmc.ca

Received 19 September 2005 / Accepted 12 January 2006

ABSTRACT

Context. About 5% of upper main sequence stars are permeated by a strong magnetic field, the origin of which is still matter of debate.
Aims. With this work we provide observational material to study how magnetic fields change with the evolution of stars on the main sequence, and to constrain theory explaining the presence of magnetic fields in A and B-type stars.
Methods. Using FORS1 in spectropolarimetric mode at the ESO VLT, we have carried out a survey of magnetic fields in early-type stars belonging to open clusters and associations of various ages.
Results. We have measured the magnetic field of 235 early-type stars with a typical uncertainty of ~100 G. In our sample, 97 stars are Ap or Bp stars. For these targets, the median error bar of our field measurements was ~80 G. A field has been detected in about 41 of these stars, 37 of which were not previously known as magnetic stars. For the 138 normal A and B-type stars, the median error bar was 136 G, and no field was detected in any of them.

Key words. stars: magnetic fields – stars: chemically peculiar – stars: evolution – polarization – techniques: polarimetric

1. Introduction

The presence of strong (~1 kG) magnetic fields in some of the A- and B-type stars of the upper main sequence has been known for more than 50 years (Babcock 1947). These fields are almost invariably associated with a suite of other unusual characteristics, which include (a) specific angular momentum of the order of 10% or less of the typical value for normal main sequence stars of similar mass; (b) quite anomalous atmospheric chemical composition, which is to first approximation a function of effective temperature (and thus is apparently an atmospheric rather than a global feature); and (c) variation of the spectrum, light and magnetic field with the star's rotational period, that clearly indicate the presence of quite significant abundance inhomogeneities and of a magnetic field not symmetric about the rotation axis.

Although considerable progress has been made in understanding the physical processes at work in these stars, many important problems remain unsolved. Among these are two major questions. First, although there is strong evidence (e.g., the stability of the observed fields, the lack of symptoms of Sun-like activity, and the lack of any important correlation of observed field strength with rotational angular velocity) that the observed fields are fossil fields, it is not yet clear how these fields evolve during the main sequence phase. Secondly, although it is believed that the basic mechanism leading to both chemical anomalies and to atmospheric inhomogeneities is the competition between gravitational settling, radiative levitation, and various hydrodynamic processes, the interplay of these processes is still very poorly understood.

In this situation, it is helpful to look to observations to guide physical theory. One kind of information about the magnetic Ap and Bp stars (hereafter referred to as magnetic

⋆ Based on observations made with ESO Telescopes at the Paranal Observatory under programme ID 068.D-0403, 070.D-0352, 272.D-5026, 073.D-0498, and 074.D-0488.
⋆⋆ Appendix is only available in electronic form at http://www.edpsciences.org

Ap stars) that has been almost entirely lacking is the age of observed stars. Good age information would be very useful for discerning systematic evolutionary changes in field strength, chemical composition, rotation rates, etc. The general lack of useful age information about magnetic Ap stars occurs because almost all of the bright magnetic Ap stars are field stars. Even with the accurate parallaxes now available from the Hipparcos mission, the uncertainties in luminosity and effective temperature of Ap stars are large enough that placing them in the HR diagram only suffices to determine very roughly their stage of evolution (see Sect. 2.1 below).

The obvious way to obtain improved ages for magnetic Ap stars is to observe such stars in open clusters. Until recently such a study has not been possible because cluster Ap stars are mostly fainter than $V \approx 6$ or 7, beyond the limit of accurate magnetic field measurements with available instruments. This situation has changed due to the development of a new generation of highly efficient spectropolarimeters and observing strategies, and their availability on large telescopes. In particular, the FORS1 spectropolarimeter on one of the ESO 8 m VLT telescopes has been shown to be a powerful tool for measuring fields in very faint Ap stars. It has recently been used to detect a field in a star of $V = 12.88$, the faintest magnetic Ap in which a field has ever been detected (Bagnulo et al. 2004).

Another very important development has been the substantial increase in the number of probable magnetic Aps identified in clusters, particularly by the systematic surveys of Maitzen and his collaborators. Furthermore, the availability of very accurate proper motions for a very large number of stars from the Hipparcos mission and the Tycho-2 catalogue has greatly facilitated the correct separation of cluster members from foreground and background stars.

The time is now clearly ripe for studying magnetic Ap stars in clusters to obtain for the first time a reasonably large sample of magnetic Ap stars of known absolute and evolutionary ages. We have started to carry out such a survey, using the FORS1 spectropolarimeter. The first stage of this survey is reported in this paper. Section 2 discusses the rationale and scope of this survey, in particular what the advantages are of studying open cluster stars compared to studying field stars, why FORS1 at the VLT is an ideal instrument for this survey, and how individual targets have been selected. Sections 3–6 describe how the magnetic field can be determined from observations of polarized spectra in terms of basic physics, observing strategy, data reduction, and $\langle B_z \rangle$ determination. These sections contain, for other FORS1 users, a detailed discussion of the optimized techniques we have developed for field measurement, and may be skipped by readers interested mainly in the observational results. In Sects. 7 and 8 we present and discuss the observations obtained during this survey. Conclusions are presented in Sect. 9.

2. The scope of this survey

2.1. Why open cluster stars?

The final goal of this series of papers will be to obtain ages, masses, and magnetic field strengths for a substantial number of Ap stars, and study whether there are evolutionary changes in the magnetic field strength. The magnetic (and sometimes the abundance) properties of a large sample of Ap stars in the field around the Sun are already known (e.g., Mathys 2004; Cowley & Bord 2004). In principle, our evolutionary study could be based on these data of field stars. To justify the need of the present survey of magnetic cluster stars we first consider the extent to which ages and masses may be derived for the stars in the field.

Temperatures for many of field stars may be estimated using available *UBV*, *uvby*, or Geneva photometry, together with calibrations provided by Stępień & Dominiczak (1989), Hauck & North (1993), and Napiwotzki et al. (1993). Luminosities require distances and bolometric corrections. Distances to many nearby Ap stars have recently been accurately determined by the Hipparcos project (see Gomez et al. 1998); for the Ap stars nearer than about 100 pc, the relative distance errors are less than about 10%. The bolometric corrections required have been discussed by Lanz (1984). Thus, it is now possible to place a large number of Ap stars on the HR diagram, and, using the evolution tracks for stars of various masses, to estimate both the mass and the age of individual stars. This exercise has been carried out by Gomez et al. (1998), by Pöhnl et al. (2005), and by Kochukhov & Bagnulo (2006) for a very large sample of nearby Ap stars, and by Hubrig et al. (2000) for a special sample of particularly slowly rotating magnetic Ap stars. In fact, as discussed below, this method is limited by large uncertainties.

Effective temperatures of magnetic Ap stars are still somewhat uncertain, more so than for normal main sequence stars because of the peculiar energy distributions of Ap stars (see Stępień & Dominiczak 1989). A recent tabulation by Sokolov (1998) of effective temperatures for nearly 70 Ap stars, with comparisons to earlier determinations, suggests that the uncertainty in $T_{\rm eff}$ typically about 5%, or ±0.02 dex.

For Hipparcos parallaxes, the distance uncertainty at 100 pc is about 8% (or about 0.035 dex), and increases with the distance itself. There is also an uncertainty in the appropriate bolometric correction (BC) to apply. First of all, there is an uncertainty of ∼0.1 mag in the estimate of the BC of a normal A-type star (due in part to the uncertainty in $T_{\rm eff}$). Then, for Ap stars, one has to apply a *correction* to the normal BC. According to Lanz (1984) this correction is uncertain by ∼0.2 mag. Finally, there is the uncertainty as to whether one should apply the Lutz-Kelker correction, about 0.1 mag at 100 pc. Taking these effects together, for nearby field stars, the uncertainty in $M_{\rm bol}$ is ∼0.3 mag, i.e., ∼0.1 dex in $\log(L/L_\odot)$. These uncertainties, once converted in the $(\log t, M/M_\odot)$ plane, correspond to age uncertainties that may be as large as half the main sequence life.

Four examples of this kind of inference are shown in the upper panel of Fig. 1, for stars of about 2.5 $M_\odot$ and 4.0 $M_\odot$, each considered for an age near the beginning of its main sequence lifetime and near the end. Comparison is made with the tracks of Schaller et al. (1992) for $Z = 0.02$. The star positions in the HR diagram, with their uncertainties (shaded boxes), are shown in the upper left panel. The deduced positions in the age-mass diagram are shown in the upper right panel. It is clear that the error boxes for observational characteristics of Ap stars translate into ages which are sufficiently uncertain that *one cannot*

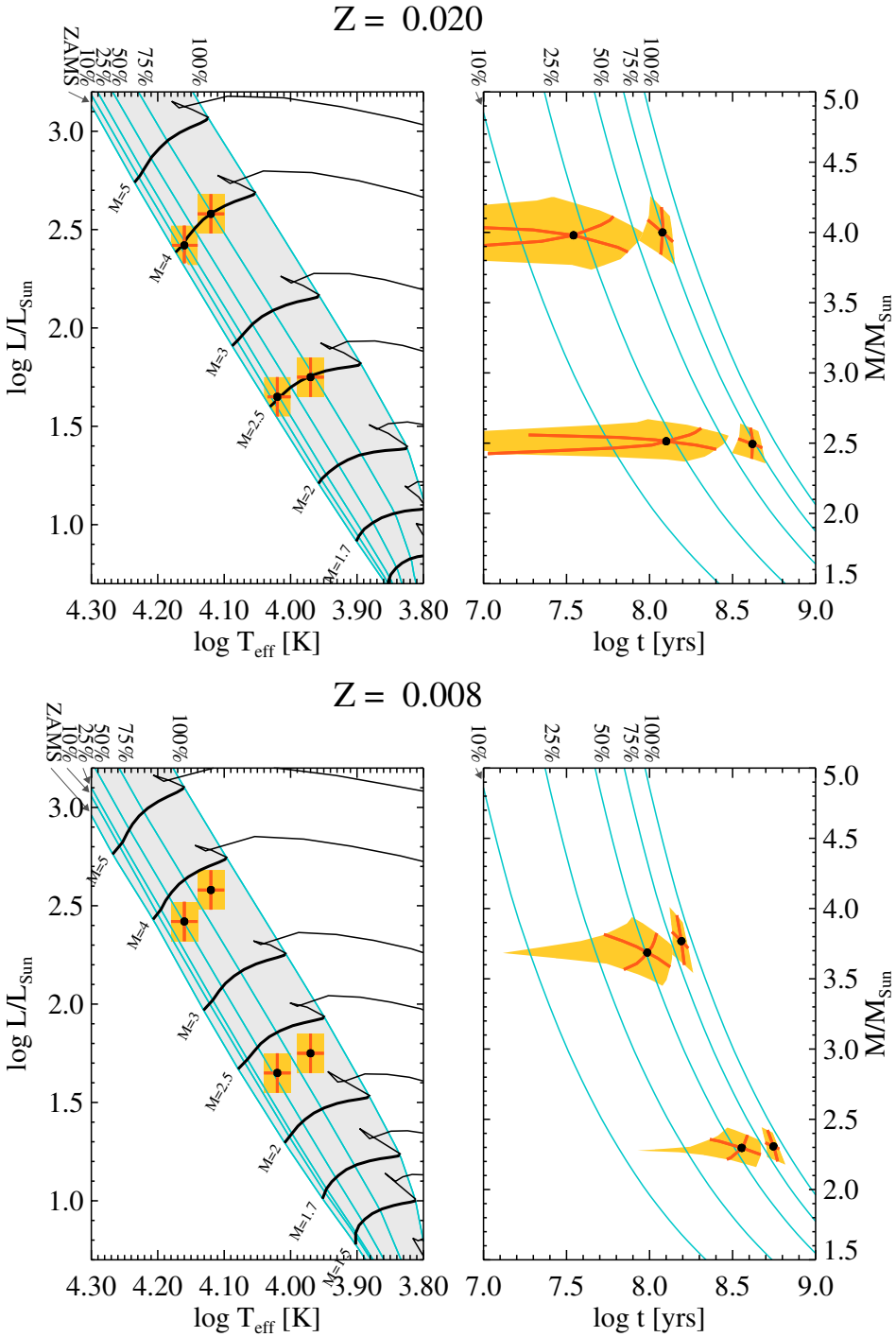

Fig. 1. Top panels: the position of a star in the HR diagram, and the star's position transformed into a diagram of age as a function of stellar mass, assuming that we know effective temperature ±5% and luminosity ±0.1 dex. The transformation uses standard evolution tracks for $Z = 0.02$ (Schaller et al. 1992); several fractional ages (fraction of main sequence life completed) are labelled. Bottom panels: the same transformation as in the top panels, but using tracks of metallicity $Z = 0.008$ (Schaerer et al. 1993).

resolve at least the first half of the main sequence lifetime. The situation is somewhat better near the end of the main sequence life, where the isochrones are farther apart, but typically an age uncertainty of the order of ±25% of the total main sequence lifetime is to be expected.

A further uncertainty in the transformation from the $(\log T_{\rm eff}, \log(L/L_\odot))$ to the $(\log t, M/M_\odot)$ plane comes from the fact that we do not know accurately the bulk chemical composition of any field Ap star, and thus we do not know what chemical composition should be assumed in the theoretical tracks used for the comparison. To estimate the size of this effect, we consider the range of abundances ([Fe/H]) present in open clusters young enough to still have Ap stars (say $\log t < 9$). Searching the WEBDA database (e.g. Mermilliod & Paunzen 2003), we found that this range is of the order of 0.4 dex. This result is confirmed by examination of the younger

clusters in the catalogue of Chen et al. (2003). This range of abundances may represent a reasonable estimate of the range of values of [Fe/H] present in nearby field stars.

A change in [Fe/H] of 0.4 dex corresponds to a change in metal abundance of about a factor of 2.5. This is just the difference in abundance between the evolution calculations with $Z = 0.008$ and $Z = 0.02$ provided by the Geneva group (Schaller et al. 1992; Schaerer et al. 1993). Repeating the transformation from the ($\log T_{\rm eff}$, $\log(L/L_\odot)$) to the ($\log t$, $M/M_\odot$) plane for $Z = 0.008$, we find the results shown in the lower panels of Fig. 1. (We have used the same values of $T_{\rm eff}$ and $\log(L/L_\odot)$ as in the upper panels.) The effect of the uncertainty in bulk chemical composition is to add roughly another ±0.25 uncertainty to the deduced fraction of the main sequence life completed by a particular star. Overall, we see that knowledge of $T_{\rm eff}$ and $\log(L/L_\odot)$ provides us with mass estimates accurate to about ±10%, but provides only poor age resolution, especially in the first half of the main sequence life (see also Fig. 4 of Kochukhov & Bagnulo 2006).

The situation is substantially improved if the star is a member of a cluster or association. The absolute age of the star is then known with essentially the precision of the cluster age. The uncertainty of this number varies from cluster to cluster, mainly because of the difficulty of deciding exactly where to place the cluster turnoff. Typically the uncertainty in $\log t$ is of the order of ±0.2 dex, about ±50% of the absolute age (see for example Castellani et al. 1992), although more accurate ages are sometimes reported (e.g. Carrier et al. 1999). This represents a very considerable improvement in absolute age, especially for a star in the early part of its main sequence life. If we know only position in the HR diagram, a star with an actual age of 10^7 yr and a main sequence lifetime of 10^9 yr would have an age uncertainty of the order of 3×10^8 yr, while the same star in a cluster would have an age uncertainty of roughly 3×10^6 yr. Only for a star in about the last third of its main sequence life is the age uncertainty not substantially improved by knowing that it is in a cluster. Another advantage of studying cluster stars is that one may determine the appropriate cluster bulk metallicity (and hence decide what evolution tracks to use for comparison) by studying the lower main sequence stars.

The masses of cluster stars can be determined with similar methods and similar (or better) accuracy than for local field stars. The values of $T_{\rm eff}$ are known with about the same accuracy as for local field stars, and there are the same uncertainties for the bolometric correction. Hipparcos parallaxes are normally not available, but the value of luminosity is obtained from the observed V magnitude together with the cluster's apparent distance modulus ($V - M_V$). Recent determinations of distance modulus by main sequence fitting appear to achieve an accuracy of about ±0.2 mag (e.g., Robichon et al. 1999). This accuracy is generally obtained out to distances well beyond those few clusters for which accurate (±25%) parallaxes are available. Furthermore, if we know the cluster metallicity, we can decide which evolution tracks to use. The precision of the mass determination of cluster stars is about ±10% if the bulk composition is not known, and somewhat better if it is.

Our conclusion is that an age derived using only the position in the HR diagram of an *individual* Ap star in the field is at present sufficiently uncertain to be of little value except for stars near the end of their main sequence lives (although important conclusions can still be drawn from statistical considerations: see Pöhnl et al. 2005 and Kochukhov & Bagnulo 2006). In contrast, if the star is a member of a cluster of known age, it is possible to determine accurately *both* the mass and age (or fraction of main sequence life elapsed). Therefore, the study of Ap stars that are cluster members is of great value in understanding the temporal evolution of rotation, magnetic fields, and atmospheric chemistry in all magnetic Ap stars.

At present only a few cluster Ap star candidates are known to be magnetic. The total number of clusters for which magnetic observations had been published is eight, with a total of 13 stars surveyed. In addition, extensive surveys had been carried in for the Ori OB1 (Borra 1981) and Sco OB2 associations (Thompson et al. 1987). Accordingly, we have decided to carry out a survey of magnetic stars in open clusters to provide age information for a substantial sample of Ap stars.

2.2. Why FORS1 at the VLT

To decide on a suitable observing strategy, we must determine what field strength we wish to detect. Among Ap stars in the local field, it appears that the median root-mean-square observed line-of-sight field strength $\langle B_z \rangle$ is of the order of 300 G (Bohlender & Landstreet 1990). We assume that this will also be typical of cluster Ap stars. In order to detect such a small value, it is important for the survey to achieve measurement uncertainties of the order of 100 G or less, as far as possible independent of the star's effective temperature and $v_{\rm e} \sin i$.

In principle, we may carry out a survey by searching either for visible Zeeman splitting of spectral lines in a simple intensity spectrum, or by searching for the circular polarization signature of a global field of simple structure. Although Mathys and collaborators (e.g., Mathys et al. 1997) have shown that Zeeman splitting may be detected in some tens of field stars, this requires quite special circumstances (i.e., $v_{\rm e} \sin i$ at most a few km s^{-1}, and field strength at least 2 kG) that are not met in most of the known magnetic Ap stars. Polarization measurement is generally a far more sensitive and broadly-applicable method of field detection than observation of Zeeman splitting.

Two main methods of measurement are currently in use for detecting the circular polarization produced by a non-zero value of $\langle B_z \rangle$. One method exploits the Zeeman polarization in metal lines (e.g., Babcock 1958; Preston & Stępień 1968; Mathys & Hubrig 1997; Wade et al. 2000; Elkin et al. 2003). Field measurement by this method usually relies on circular spectropolarimetry with a resolving power $R \geq 3 \times 10^4$. If the star is quite bright, with a $v_{\rm e} \sin i$ value smaller than, say, 15 or 20 km s^{-1} and a rich spectrum, field errors σ_B as small as a few G can be achieved (Shorlin et al. 2002). On the other hand, the measurement uncertainty depends strongly on spectral type (which determines the number of usable lines and their intrinsic depths) and on $v_{\rm e} \sin i$. In observations collecting similar total numbers of photons, the standard error of field measurement can vary by a factor of order 10^2.

A second method employs the Zeeman polarization in the wings of the Balmer lines. These lines may be observed with quite low resolving power ($R \sim 10^3$), using either interference filters (e.g., Borra & Landstreet 1980) or a low-dispersion spectrograph (Bagnulo et al. 2002). Since the Balmer lines are intrinsically broad, the polarization signal may be a factor of 10 smaller than in the metal lines, and the best achievable standard errors are of order 30–50 G (Landstreet 1982). However, since the Balmer lines are always quite deep, and do not vary much in strength among A and B stars, and since the overall profile at $R \approx 10^3$ is hardly affected by rotation, this method can provide standard errors that are fairly uniform simply by surveying a sample of stars to a specified signal-to-noise ratio.

The (spectro-)polarimeters now in use make both kinds of field measurement. However, limitations imposed by low overall efficiency and (usually) modest telescope aperture have limited most of the $\langle B_z \rangle$ field measurements to stars not much fainter than $V = 6$. This magnitude limit has effectively prevented any serious survey of magnetic fields in cluster Ap stars, as only a handful of clusters and associations have a significant number of Ap stars brighter than $V = 6$. With a limiting magnetic around $V = 6$, one is restricted to clusters and associations not much more than 100 pc away, since the absolute magnitude of an Ap star is typically in the range of $M_V \sim -1$ to $+1$. Only half a dozen clusters are this near.

The development of the FORS1 spectropolarimeter for the ESO Very Large Telescope (VLT) has changed the situation dramatically. FORS1 incorporates a multi-object low dispersion spectrograph with polarizing optics. In polarimetric mode, spectra with $R \sim 10^3$ may be obtained for up to nine objects simultaneously in a field $7'$ square. Bagnulo et al. (2002) have shown that FORS1 can be used very effectively as a Balmer-line polarimeter for field measurement. Since this instrument is mounted on an 8 m telescope, and has a very high throughput, the limiting magnitude is much fainter than with earlier instruments. Bagnulo et al. (2004) have used FORS1 to detect a field in a star of $V \approx 13$ in 2.8 h of observation, and showed that it is possible to reach a precision of $\sigma_B \sim 10^2$ G in about 1 h of integration at $V = 10$. With a limiting magnitude of 10 or even fainter, we can survey clusters and associations out to several hundred pc, and the number of clusters that can be studied rises to roughly 100. In addition Bagnulo et al. (2002) have shown that the low resolution does not prevent the use of metal lines to measure the magnetic field in stars with rich metallic spectra. This fact may be used to increase the sensitivity of field measurements in some stars. A third advantage of FORS1 is that in clusters, it is often possible to observe several stars simultaneously. We have used this capability to observe multiple Ap candidate stars, but also non-Ap cluster members in the hopes of making serendipitous field detections.

This survey is biased toward stars with longitudinal field of absolute value larger than about 200–300 G, but is not biased with respect to $v \sin i$. Any bias with respect to spectral type is primarily a feature of the previous classification programmes that have identified candidate magnetic Ap stars in clusters, rather than a feature imposed by an instrumental field detection sensitivity that depends on the star's spectroscopic features.

2.3. The target list

Two problems arise in the selection of a list of suitable targets for a survey of magnetic fields in cluster stars: (a) identification of candidate Ap stars in the field of individual clusters (most of the known Ap stars are field stars) and (b) determination of cluster membership.

Numerous studies have identified probable Ap members of clusters and associations. Surveys for Ap/Bp cluster members based on low-dispersion spectroscopy were reported by Hartoog (1976, 1977), and by Abt (1979). Probable Ap stars have also been reported from a number of studies of individual clusters (e.g. Dachs & Kabus 1989). Furthermore, the Michigan Spectral Survey (e.g. Houk & Smith-Moore 1988) has provided uniform MK classifications for a large number of HD stars in the fields of clusters south of $\delta = +5°$. This allowed us to select some Ap stars that are possible cluster members.

Another important source of identifications of cluster Ap stars has been the use of photometric indices that are sensitive to a broad depression near 5200 Å in the energy distribution of most Ap stars (e.g., Kupka et al. 2003). In particular, Maitzen and collaborators (e.g., Maitzen 1993) have developed a narrow band photometric index (Δa) which is reasonably sensitive to the spectral peculiarities of Ap stars with effective temperatures in the range ~8000–14 000 K. Maitzen's group has systematically obtained Δa photometry of many clusters to identify Ap stars. The Δa system has also been used by Joncas & Borra (1981) to search for Ap stars in the Orion OB1 association.

It is also known that the Z index, which can be computed for the many cluster stars for which Geneva photometry is available, is a powerful discriminant of Ap stars in approximately the same temperature range as the Δa index (e.g. Kramer & Maeder 1980; Hauck & North 1982).

We have made extensive use of the WEBDA cluster database (e.g. Mermilliod & Paunzen 2003), Simbad, and a catalogue of candidate cluster Ap stars by Renson (1992).

Most of the surveys discussed above have made a serious effort to determine cluster memberships, mainly on the basis of spatial location and apparent magnitude. However, recent work based on and stimulated by the Hipparcos astrometric space mission has led to a major expansion in the available data on parallaxes and proper motions. Hipparcos parallaxes (e.g. Gomez et al. 1998) provide a valuable membership discriminant out to about 300 pc for many cluster stars. Even more importantly, the Tycho (Høg et al. 1998) and Tycho-2 (Høg et al. 2000) proper motion catalogues now provide powerful tests of membership out to nearly one kpc, for a much larger number of stars, as demonstrated for example by Robichon et al. (1999), de Zeeuw et al. (1999), and Dias et al. (2001).

Using the resources discussed above, a database containing a variety of information on more than 200 suspected Ap cluster members in more than 70 clusters and associations was constructed and used for the selection of the targets. In general, we have given highest priority to stars which appear to be probable Ap stars, and probable cluster members, but we have also observed a number of stars for which at least one of these criteria was uncertain. Up to the present time, we have been able

to observe (or occasionally find in the literature) magnetic observations of about 1/3 of the stars in our database.

Cluster membership will be discussed in the second paper in this series (Landstreet et al., in preparation, hereafter referred to as Paper II), where we will analyze the astrophysical and evolutionary results of our survey in more detail. The present paper focuses on the magnetic observations themselves.

3. The basic formulae

The diagnostic tool for stellar magnetic fields used in this work has been proposed by Bagnulo et al. (2002). Here we review and elaborate this method.

The *mean longitudinal magnetic field* $\langle B_z \rangle$, i.e., the component of the magnetic field along the line of sight averaged over the visible stellar disk, can be measured through the analysis of the circular polarization of spectral lines. In the *weak field* regime (i.e., when the Zeeman splitting is small compared to the line intrinsic broadening) we have (e.g. Landstreet 1982)

$$\frac{V}{I} = -g_{\rm eff}\, C_z\, \lambda^2\, \frac{1}{I}\, \frac{{\rm d}I}{{\rm d}\lambda}\, \langle B_z \rangle, \tag{1}$$

where $g_{\rm eff}$ is the effective Landé factor (1 for H Balmer lines, see Casini & Landi Degl'Innocenti 1994), V is the Stokes parameter which measures the circular polarization, I is the total (unpolarized) intensity, λ is the wavelength expressed in Å, $\langle B_z \rangle$ is the longitudinal field expressed in Gauss, and

$$C_z = \frac{e}{4\pi m_{\rm e} c^2} \quad \left(\simeq 4.67 \times 10^{-13}\ {\rm \AA}^{-1}\ {\rm G}^{-1}\right) \tag{2}$$

where e is the electron charge, $m_{\rm e}$ the electron mass, and c the speed of light. For a typical A-star atmosphere, the weak-field approximation holds for field strength $\lesssim$1 kG for metal lines, and up to ~10 kG for H lines.

A least-squares technique can be used to derive the longitudinal field via Eq. (1). We minimise the expression

$$\chi^2 = \sum_i \frac{(y_i - \langle B_z \rangle\, x_i - b)^2}{\sigma_i^2} \tag{3}$$

where, for each spectral point i, $y_i = (V/I)_i$, $x_i = -g_{\rm eff} C_z \lambda_i^2 (1/I \times {\rm d}I/{\rm d}\lambda)_i$, and b is a constant. For each spectral point i, the derivative of Stokes I with respect to wavelength is evaluated as

$$\left(\frac{{\rm d}I}{{\rm d}\lambda}\right)_{\lambda=\lambda_i} = \frac{\mathcal{N}_{i+1} - \mathcal{N}_{i-1}}{\lambda_{i+1} - \lambda_{i-1}} \tag{4}$$

where $\mathcal{N}_i$ is the photon count at wavelength λ_i. The estimates for the errors on the parameters $\langle B_z \rangle$ and b are given by the diagonal elements of the inverse of the χ^2 matrix (see, e.g., Bevington 1969).

The application of a least-squares technique is justified if

$$\langle B_z \rangle\ \sigma_{x_i} \ll \sigma_{y_i} \tag{5}$$

(see, e.g., Bevington 1969), where

$$\sigma_{x_i}^2 = \left(-g_{\rm eff}\, C_z\, \lambda_i^2\right)^2 \left(\left(-\frac{1}{I^2}\right)^2 \left(\frac{{\rm d}I}{{\rm d}\lambda_i}\right)^2 \sigma_I^2 + \left(\frac{1}{I}\right)^2 \sigma_{{\rm d}I/{\rm d}\lambda}^2\right) \tag{6}$$

and

$$\sigma_{y_i}^2 = \sigma^2\, [(V/I)_i]\,.$$

For the stars studied in this work, we have verified that, at all observed wavelengths, Eq. (5) is verified.

4. Instrument and instrument setup

The Focal Reducer/Low Dispersion Spectrograph FORS1 of the ESO VLT is a multi-mode instrument equipped with polarimetric optics. The instrument characteristics and performances are outlined by Seifert et al. (2000) and in the FORS1/2 User Manual (VLT-MAN-ESO-13100-1543). In this survey FORS1 has been used as a low resolution spectropolarimeter.

4.1. Instrument mode

Spectropolarimetry with FORS1 can be performed in two different observing modes: *fast mode* and *fims mode*. *Fast mode* is used for observations of individual objects that can be acquired "fast" with a simple centering on the slit. *Fims* mode permits one to place slitlets on up to nine targets within a $6.8' \times 6.8'$ field of view (multi-object spectropolarimetry). Whenever our main targets were in a field including other stars of similar magnitude, we observed in *fims mode*. In this way, in addition to polarized spectra of Ap stars, we obtained polarized spectra of numerous normal A and B-type cluster stars.

4.2. Grism choice

We have used the grisms 600 B and 600 R, which cover the spectral ranges 3450–5900 Å, and 5250–7450 Å, respectively. Grism 600 B covers all H Balmer lines from Hβ down to the Balmer jump; grism 600 R covers Hα. Both grisms have 600 grooves mm^{-1}, and yield dispersions of 1.20 Å, and 1.08 Å per pixel, respectively. With a 1″ slit width they provide spectral resolving powers of 780 and 1160, respectively.

For this study, grism 600 B seems a better choice than 600 R. Although Hα is more sensitive to the magnetic field than individual H Balmer lines at shorter wavelengths (the Zeeman effect depends quadratically upon wavelength), the combined analysis of several Balmer lines from Hβ down to the Balmer jump leads to a smaller error bar than the analysis of Hα only. Furthermore, the flux of an A-type stars is larger in the blue than in the red, therefore the same SNR can be reached with a shorter integration time using grism 600 B rather than grism 600 R. On the other hand, it should be noted that the useful field of view in *fims mode* depends on the spectral range that one wishes to cover: the larger the spectral range that one needs to observe, the smaller the spatial region where one can place slitlets. Hence, in *fims mode*, grism 600 R offers more flexibility than grism 600 B, as its useful wavelength coverage corresponds to Hα only, which does not put a strong constraint on the field of view. In (ESO period) P68 we used grism 600 R (in combination with the order separation filter GG 435). In P70, P72, P73, and P74, we used grism 600 B (with no order separation filter).

For most of the observations, we have used a slit width of 0.5″ or 0.8″.

4.3. CCD readout

In polarimetric mode, overheads represent a significant fraction of the total telescope time. Ultra-high SNR observations (needed to reach the wanted uncertainty of ∼100 G) require multiple exposures, hence, multiple CCD readouts. We minimized the CCD readout time as follows. In case of observations of individual stars (*fast mode*) we used a windowed read-out mode of 2048 × 400 pixels. In case of multi-object observations (*fims mode*) where the full size of the CCD was needed, we used a 4-port readout. The lowest available gain was selected, as to maximise the actual electron capacity, hence, the SNR that can be reached with each single exposure.

5. Data reduction

5.1. Frame pre-processing, spectrum extraction and wavelength calibration

The data have been reduced and optimally extracted using standard IRAF routines. All the science frames have been bias subtracted with the corresponding master bias obtained from a series of five frames taken the morning after the observations. No flat fielding procedure has been applied to our data. By performing reduction experiments with and without flat-fielding, we have verified that flat fielding does not influence significantly the final computation of the Stokes profiles. In fact, flat fields obtained with the grism 600 B are severely affected by internal reflections from the Longitudinal Atmospheric Dispersion Corrector (LADC). Frames obtained in *fims mode* were read out in four ports. The CCD is thus divided in four quadrants, each of them characterized by its own bias level and gain. In order to compensate for the different gains, we multiplied each science frames by the ratio of an imaging screen flat read out in one port and an imaging screen flat read out in four ports.

When extracting the spectra we found that the use of standard extraction apertures (∼10 pixels width) introduced artefacts into the Stokes V spectrum. This problem was solved using apertures as large as ∼4−5 times the spatial FWHM of the spectrum, i.e., typically 50 pixels width. Apertures that are not symmetric about the flux peak have been used for stars close to the edge of the slit. This occurred occasionally for targets observed in *fims mode*. We used a high-order (∼15) Legendre fitting function to trace the spectrum[1]. Lower order functions were used only in the case of low SNR secondary targets (typically in frames obtained in *fims mode*) and/or in the case of spectra the length of which occupied just a fraction of the CCD (again in *fims* frames, depending on the positioning of the slitlets).

Sky subtraction was performed differently for spectra obtained in *fast* and *fims mode*. In the first case the sky subtraction was performed selecting symmetric regions on the left and right side of each spectrum (typically between pixel 40 and 50 from the central peak), and fitting those with a Chebyshev polynomial. In the case of data obtained in *fims mode*, whenever the star was not positioned at the center of the slitlet, the sky was estimated on just one region at one side of the spectrum. In fact, we found that sky-subtraction is not critical in the sense that it does not significantly affect the final results. In some cases, we preferred not to perform sky-subtraction at all, because of the presence of LADC reflections close to the spectrum.

The FORS1 calibration plan includes wavelength calibrations frames obtained at all retarder waveplate positions used for the science. However, we found that the best and safest strategy is to use, for a complete set of science data, just a single wavelength calibration frame, and not match science and wavelength calibration frames according to their retarder waveplate angles. We found that this latter method occasionally introduces spurious polarization signals.

Wavelength calibration typically led to RMS scatter of ∼0.1 pixels and maximum error of ≤20 km s^{-1}. The fine tuning of wavelength calibration based on night sky lines could not be performed. Therefore the accuracy of the wavelength calibration is restricted by instrument flexures, which are expected to be less than 1 pixel up to a zenith distance of 60° (see FORS1/2 User Manual). Numerical tests show that this is of negligible impact on the determination of the mean longitudinal magnetic field, using the method described by Bagnulo et al. (2002) and elaborated below.

5.2. Obtaining stokes V

Circular polarization measurements are performed by inserting the quarter-wave plate and the Wollaston prism into the optical path. A combination of exposures taken at different waveplate orientations allows one to minimise the contributions of spurious (instrumental) polarization. The FORS user manual explains that instrumental polarization cancels out to the first order if Stokes V is obtained from

$$\frac{V}{I} = \frac{1}{2}\left\{\left(\frac{f^{\rm o}-f^{\rm e}}{f^{\rm o}+f^{\rm e}}\right)_{\alpha=-45^\circ} - \left(\frac{f^{\rm o}-f^{\rm e}}{f^{\rm o}+f^{\rm e}}\right)_{\alpha=+45^\circ}\right\}, \quad (7)$$

where $f^{\rm o}$ and $f^{\rm e}$ are the ordinary and extraordinary beams, respectively, and α is the position angle of the retarder waveplate (in fact, note that the FORS1/2 manual gives the formula with the opposite sign). Another possibility is to obtain Stokes V from

$$\frac{V}{I} = \frac{r-1}{r+1} \quad (8)$$

where

$$r^2 = \frac{(f^{\rm o}/f^{\rm e})_{\alpha=-45^\circ}}{(f^{\rm o}/f^{\rm e})_{\alpha=+45^\circ}}$$

(e.g., Donati et al. 1997). We have verified that Eqs. (7) and (8) give consistent results both for Stokes V and $\langle B_z \rangle$.

[1] The high order of the fitting function is justified by the high SNR that makes it possible to trace very accurately the spectrum across the CCD.

The error bar associated with the Stokes V/I, computed via Eq. (7) is

$$\sigma^2\left[(V/I)\right] = \left(\left(\frac{f^{\rm e}}{(f^{\rm o}+f^{\rm e})^2}\right)^2\sigma^2_{f^{\rm o}} + \left(\frac{f^{\rm o}}{(f^{\rm o}+f^{\rm e})^2}\right)^2\sigma^2_{f^{\rm e}}\right)_{\alpha=-45^\circ} + \left(\left(\frac{f^{\rm e}}{(f^{\rm o}+f^{\rm e})^2}\right)^2\sigma^2_{f^{\rm o}} + \left(\frac{f^{\rm o}}{(f^{\rm o}+f^{\rm e})^2}\right)^2\sigma^2_{f^{\rm e}}\right)_{\alpha=+45^\circ}. \quad (9)$$

Equation (9) can be simplified as follows. Let us assume

$$\left(\sigma^2_{f^{\rm o}}\right)_{\alpha=\pm45^\circ} = \left(\sigma^2_{f^{\rm e}}\right)_{\alpha=\pm45^\circ} = \left(f^{\rm o}\right)_{\alpha=\pm45^\circ} = \left(f^{\rm e}\right)_{\alpha=\pm45^\circ} = \mathcal{N}$$

where $\mathcal{N}$ is an estimate of the photon count in a given wavelength range. For m pairs of observations (i.e., one exposure at $\alpha = 45^\circ$, and one exposure at $\alpha = -45^\circ$, repeated m times), Eq. (9) becomes

$$\sigma^2\left[(V/I)\right] = \frac{1}{4m\,\mathcal{N}}. \quad (10)$$

Equation (10) simply states that the error bar on V/I decreases as $1/\sqrt{\mathcal{N}}$. The polarization in a given wavelength range can be measured with an 0.1% uncertainty if at least 2.5×10^5 photons are accumulated both in the ordinary and in the extraordinary beam, and in each of the two exposures of a pair.

In order to detect weak magnetic fields ($\lesssim$300 G) with the technique used in this work, one has to obtain ultra high SNR ($\gtrsim$1500 Å^{-1}) observations. Even with a 8 m telescope, this can be achieved only on relatively bright stars ($V \lesssim 13$, if we limit the shutter time to $\lesssim$2 h). Due to the limited CCD well capacity, multiple exposures have to be taken. From a practical point of view, one has to set the exposure time to a value that maximises the photon count without risk of CCD saturation (e.g., by adjusting the exposure time to get a peak count of 30 000 ADU per pixel), and then take several pairs of exposures with the retarder waveplate at the +45° and −45° positions. Equation (10) can be explicitly expressed in terms of ADU in the following way. Let us define M as the ADU per pixel and g as the number of electrons per ADU, so that actual photon count $\mathcal{N}$ is given by gM. Let us also define $\mathcal{A}_{\rm s}$ as the ratio between the ADU integrated in a pixel column along the direction perpendicular to the dispersion, and the peak ADU in the central pixel. The error bar on the circular polarization measured in the wavelength interval $\Delta\lambda$ covered by 1 pixel is given by

$$\sigma^2\left[(V/I)\right](\Delta\lambda) = \frac{1}{4\,m\,g\,\mathcal{A}_{\rm s}\,M_{\rm max}}$$

where $M_{\rm max}$ is the peak ADU.

Recalling the properties of a Gaussian, we can write $\mathcal{A}_{\rm s} = 1.065\,{\rm FWHM}$. With a plate scale of 0.2″ per pixel, as in the case of FORS1, and with 0.8″ seeing, $\mathcal{A}_{\rm s} \simeq 4$. Assuming $g = 2.9$ (a typical value for the FORS1 "low gain" readout mode), and setting as a peak value $M_{\rm max} = 30\,000$ ADU, we get

$$\sigma\left[(V/I)\right](\Delta\lambda) \simeq 8\times10^{-4}\,\frac{1}{\sqrt{m}}. \quad (11)$$

Equation (11) allows one to calculate the number of pairs of exposures that are needed to measure V/I with a given error bar. For instance, with a pair of exposures at half the CCD full well, one gets an error bar close to 0.1%. To go below the threshold of an 0.01% error bar (if possible at all) one should obtain 64 pairs of exposures.

We found that measuring V/I with an accuracy of a few units in 10^{-4} per Å in the continuum near to Hβ allowed us to measure magnetic fields with an error bar between 50 and 100 G. Therefore, we decided that our observing strategy would be based on a series of four pairs of exposures (following the sequence $\alpha = +45^\circ, -45^\circ, -45^\circ, +45^\circ$, etc.). However, we could limit the number of pairs of exposure to four only when we obtained telescope time in visitor mode, which allowed us to optimize the exposure time based on the weather conditions. During P72 and P73 we were allocated telescope time in service mode, and were forced to set the exposure time to conservatively low values to be sure to avoid CCD saturation. In these cases the number of pairs of exposures was increased from four to six or eight to guarantee a sufficient SNR.

Thought must be given to the ratio between shutter time and overhead time, as the latter (~20 min for a series of 4 pairs of exposures) may represent a substantial fraction of the total time for a single pointing. Using grism 600 B with a 0.5″ slit width, we can obtain a peak ADU count of ~30 000 in about 10 min shutter time for a $V = 11-12$ A-type star (depending on the weather conditions), and in just 1 min for $V = 8.5-9.5$.

5.3. The use of a σ-clipping algorithm

The simplest method to obtain V/I is to add up all spectra obtained in the same beam and with same retarder waveplate position, and then use Eq. (7). However, reduction products can be improved by using a σ-clipping algorithm as follows. For each wavelength step one calculates

$$\left(\frac{V}{I}\right)_{ij} = \frac{1}{2}\left\{\left(\frac{f^{\rm o}_i - f^{\rm e}_i}{f^{\rm o}_i + f^{\rm e}_i}\right)_{\alpha=-45^\circ} - \left(\frac{f^{\rm o}_j - f^{\rm e}_j}{f^{\rm o}_j + f^{\rm e}_j}\right)_{\alpha=+45^\circ}\right\} \quad i,\,j = 1, 2, \ldots, m \quad (12)$$

where m is the total number of pairs of observations. Then, one calculates the median $\widehat{(V/I)}$ from the m^2 $(V/I)_{ij}$ values, and the median absolute deviation (MAD), i.e., the median of the distribution

$$\left|\left((V/I)_{ij} - \widehat{(V/I)}\right)\right|.$$

Setting $\sigma = 1.48\,{\rm MAD}$ (e.g., Huber 1981, pp. 107–108), those $(V/I)_{ij}$ values for which

$$|(V/I)_{ij} - \widehat{(V/I)}| > \mathcal{K}\sigma$$

are rejected (we typically adopted $\mathcal{K} = 3$). The procedure is iterated until no points are rejected, but from the second iteration on, the median $\widehat{(V/I)}$ is replaced by the weighted average

$$\overline{(V/I)} = \sum_{ij}(V/I)_{ij}\,\sigma^{-2}[(V/I)_{ij}] \;/\; \sum_{ij}\sigma^{-2}[(V/I)_{ij}], \quad (13)$$

where the sum is obviously extended over the K $(V/I)_{ij}$ values that have not been rejected by the σ-clipping algorithm ($K \leq m^2$), and $\sigma^2\left[(V/I)_{ij}\right]$ is given by Eq. (9).

Table 1. $\langle B_z \rangle$ measurements of the $V = 6.1$ Ap star HD 94660 = KQ Vel. Date, UT, and signal to noise ratio (SNR) are calculated as explained in the caption of Table A.3. Observations obtained in P66 had been already published by Bagnulo et al. (2002).

Period	DATE	UT	$\langle B_z \rangle$ (G) Balmer lines	$\langle B_z \rangle$ (G) metal lines	$\langle B_z \rangle$ (G) full spectrum	SNR	Grism
P66	2001-03-22	23:54:00	-2085 ± 85	-2100 ± 100	-2260 ± 65	1550	600 B
P68	2002-02-04	08:43:13	-2335 ± 57	-2141 ± 52	-2226 ± 37	2100	600 B
P68	2002-02-04	08:56:09	-2083 ± 75	-2516 ± 34	-2439 ± 31	2150	600 R
P70	2003-02-08	09:41:49	-2574 ± 57	-2051 ± 48	-2260 ± 38	2150	600 B
P74	2005-01-30	09:33:45	-2432 ± 50	-2002 ± 43	-2190 ± 32	2300	600 B

If no value in the m^2 set of $(V/I)_{ij}$ pairs has been rejected, and if we assume that the errors given by Eq. (9) are approximately equal for all spectra, we can estimate the error bar of $\overline{(V/I)}$ as:

$$\left\{\sigma^2\left[\overline{(V/I)}\right]\right\}' \simeq \frac{1}{m}\sigma^2\left[(V/I)\right]. \quad (14)$$

An alternative estimate of the same error bar can be obtained as follows:

$$\left\{\sigma^2\left[\overline{(V/I)}\right]\right\}'' \simeq \frac{1}{m^2(m-1)}\sum_{ij}[(V/I)_{ij} - \overline{(V/I)}]^2. \quad (15)$$

In practice, at each wavelength step, we adopt the error bar given by the maximum among the values obtained from Eqs. (14) and (15). The above two expressions will be derived in detail in Appendix A, together with more general expressions valid for the case of one or more exposures rejected by the σ-clipping algorithm.

5.4. Measuring $\langle B_z \rangle$

The mean longitudinal field $\langle B_z \rangle$ is obtained as explained in Sect. 3, using V/I obtained via Eq. (13). Following common statistics guidelines, one should consider a detection as "definite" whenever the relation

$$|\langle B_z \rangle| / \sigma\left[\langle B_z \rangle\right] \geq 3 \quad (16)$$

is satisfied.

We encountered a number of cases for which the field was detected at about 3-σ level, and where minor changes in the data reduction would transform a marginal detection in a null or in a definite detection. Although these cases should certainly be investigated via additional observations, we tried to extract further information from the available spectra, to formulate a more robust and reliable criterion for field detection.

First, we decided to explore an alternative method for the determination of the mean longitudinal field. From the individual pairs of V_{ij}/I_{ij} and I_{ij} given by Eqs. (12), we calculated m^2 $\langle B_z \rangle_{ij}$ values, and the weighted mean longitudinal field

$$\langle B_z \rangle' = \sum_{ij}\langle B_z \rangle_{ij}\,\sigma^{-2}\left[\langle B_z \rangle_{ij}\right] / \sum_{ij}\sigma^{-2}\left[\langle B_z \rangle_{ij}\right]. \quad (17)$$

The corresponding error bar $\sigma\left[\langle B_z \rangle'\right]$ was calculated as

$$\sigma^2\left[\langle B_z \rangle'\right] = \frac{\sum_{ij=1}^{m}(\langle B_z \rangle_{ij} - \langle B_z \rangle')^2}{m^2(m-1)}.$$

For each star, we systematically checked the consistency between the $\langle B_z \rangle$ value determined through the average V/I obtained via Eq. (13) and the $\langle B_z \rangle'$ value obtained via Eq. (17). We also checked whether the relation

$$|\langle B_z \rangle'| / \sigma\left[\langle B_z \rangle'\right] \geq 3 \quad (18)$$

was satisfied.

Second, we performed a systematic analysis of metal lines. As pointed out earlier, Eq. (1) is formally valid only under the weak-field approximation. Therefore, in principle, $\langle B_z \rangle$ measurements by our method should be performed only on H Balmer lines. Furthermore, H Balmer lines are well sampled even at the low resolution of our observations, whereas metal lines are unresolved. Nevertheless, we found that the $\langle B_z \rangle$ determined via metal line analysis is consistent with that measured from H Balmer lines, provided that $\langle B_z \rangle$ is $\lesssim$800 G (see Sect. 6.2). Therefore we decided to analyze the metal lines, i.e., to apply the least-squares technique to spectral regions free from H Balmer lines. In addition, we determined $\langle B_z \rangle$ using the whole spectrum, i.e., including both Balmer and metal lines. The outcome of this analysis will be discussed in Sect. 6.

6. Magnetic field determinations from Balmer lines vs. field determinations from metal lines

6.1. The magnetic "standard" star HD 94660

In order to compare our results with those obtained through different techniques, we repeatedly observed a well known magnetic Ap star: HD 94660 (=KQ Vel). Previous $\langle B_z \rangle$ measurements of HD 94660 were obtained using the Hα Balmer line (Borra & Landstreet 1975), the Hβ Balmer line (Bohlender et al. 1993), and metallic lines (Mathys 1994; Mathys & Hubrig 1997). Moreover, HD 94660 is the star observed by Bagnulo et al. (2002) to develop the technique used in this work.

The log of our observations and $\langle B_z \rangle$ measurements is given in Table 1. Note that on 2002-02-04 we obtained two consecutive $\langle B_z \rangle$ measurements: the first one with grism 600 B, the second one with grism 600 R.

Figure 2 shows the $\langle B_z \rangle$ measurements obtained from both the Balmer and the metal lines. The $\langle B_z \rangle$ values obtained from the Balmer lines blueward of Hβ are consistent among themselves, and marginally consistent with the $\langle B_z \rangle$ value obtained from Hα. With the exception of the measurement taken on 2001-03-22, the $\langle B_z \rangle$ values obtained from the metal lines are not consistent with those obtained from Balmer lines. This is probably due to the fact that Eq. (1) is valid only under the

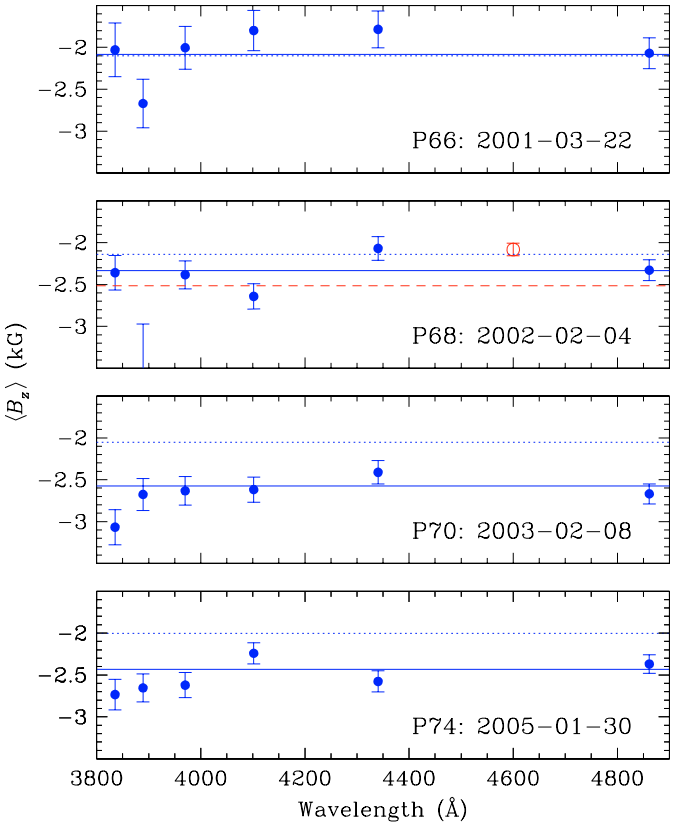

Fig. 2. $\langle B_z \rangle$ measurements of HD 94660 from individual Balmer lines. Each panel refers to a different observing date as specified in the figure. The $\langle B_z \rangle$ values measured from Hβ and blueward Balmer lines are plotted with filled circles at the corresponding wavelength. The $\langle B_z \rangle$ determination from Hα obtained on 2002-02-04 is arbitrarily plotted with an empty circle at $\lambda = 4600$ Å. The solid lines correspond to $\langle B_z \rangle$ obtained using all Balmer lines from Hβ down to the Balmer jump, and the dotted lines indicate $\langle B_z \rangle$ obtained from the metal lines with grism 600 B. The dashed line in the second panel shows the $\langle B_z \rangle$ value obtained from the metal lines observed with grism 600 R.

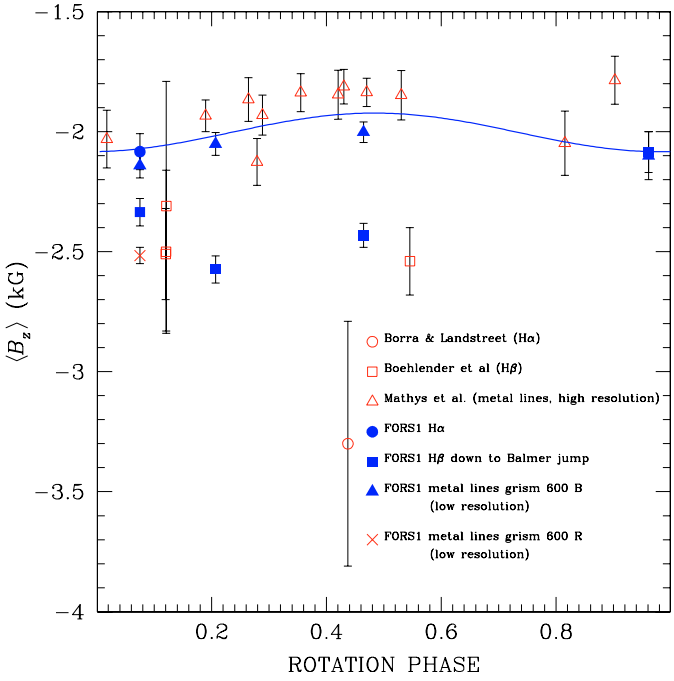

Fig. 3. Longitudinal field determinations of HD 94660. The solid line is a fit to the $\langle B_z \rangle$ determinations from metal lines. We have used a first-order Fourier expansion. At phase 0.075 we have considered the $\langle B_z \rangle$ determination obtained with grism 600 B and not the one obtained with grism 600 R. For the star's rotation period we adopt 2800 d (Landstreet & Mathys 2000), and the zero phase point is at JD = 2446500.0.

weak field approximation (which in this case is correct for Balmer lines but not for metal lines). Note also that the $\langle B_z \rangle$ values measured via metal line analysis are not consistent among themselves if we compare data obtained with grism 600 B and grism 600 R. The comparison between $\langle B_z \rangle$ values obtained from H Balmer lines and metal lines will be further discussed in Sect. 6.2.

We also compared our $\langle B_z \rangle$ determinations of Table 1 with those previously obtained in the literature, adopting for the star's rotation period 2800 d (Landstreet & Mathys 2000). The results are shown in Fig. 3. In general, it appears that $\langle B_z \rangle$ values obtained from Balmer lines are *not* consistent with the $\langle B_z \rangle$ determinations obtained using metallic lines. It seems likely that different methods used to evaluate $\langle B_z \rangle$ bear systematic differences (even though each may be internally consistent). Systematic inconsistencies between $\langle B_z \rangle$ determinations in Ap stars obtained with different chemical elements or with different techniques have been already found in previous works (see, for instance, Ryabchikova et al. 2005, who analysed several observations of HD 24712).

6.2. Weak field Ap stars

Using all our data collected for Ap stars, we show here that the metal line analysis and the Balmer line analysis produce consistent results when the weak field hypothesis is satisfied.

Figure 4 shows the $\langle B_z \rangle$ values obtained from metal lines versus those obtained from Balmer lines for the observed Ap stars. It appears that the two methods give consistent $\langle B_z \rangle$ values for $|\langle B_z \rangle| \lesssim 800$ G. Above the 1 kG level, differences between Balmer line and metal line technique become noticeable or even striking. E.g., for HD 310187 we obtained from the Balmer lines $\langle B_z \rangle = 6519 \pm 55$ G, and from the metal lines we obtained $\langle B_z \rangle = 3784 \pm 59$ G. In general, above the 1 kG level, the modulus of $\langle B_z \rangle$ determined from Balmer lines is larger than that from the metal lines, as we would expect from the earlier breakdown of the weak field expression for metal lines.

Summarizing, it appears that if the field is weak, both methods are consistent, and each gives an indication whether the star is magnetic or not *independent* of the other.

Figure 5 compares the distributions of the error bars for $\langle B_z \rangle$ obtained via Balmer and metal line analysis for the observed Ap stars. We see that the distribution of the error bars calculated via metal line analysis is broader than that obtained from Balmer lines. This is due primarily to the fact that Balmer lines have similar strength in all A and B-type stars, whereas metal lines may change greatly from star to star. For a given SNR, the error bars obtained via metal line analysis are smaller in spectra that are richer in metal lines than in spectra that are poorer in metal lines. As expected, for a set of observations

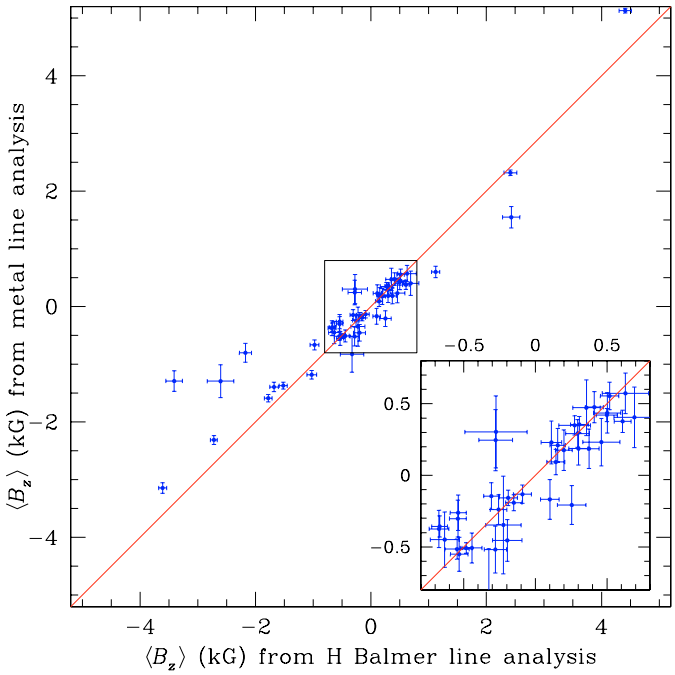

Fig. 4. $\langle B_z \rangle$ determinations from metal lines versus $\langle B_z \rangle$ determinations from Balmer lines for the stars of Table A.3. The solid line has slope = 1. For clarity, only stars for which $\langle B_z \rangle$ obtained from Balmer lines is such that $|\langle B_z \rangle|/\sigma[\langle B_z \rangle] \geq 1$ have been plotted. The outliers HD 318107 and NGC 2244 334 (see Table A.3) are not plotted.

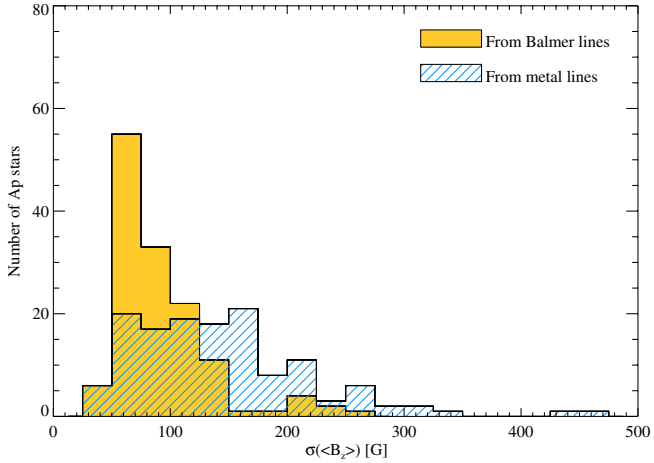

Fig. 5. Histograms of the error bars for the $\langle B_z \rangle$ measurements of Table A.3 obtained from Balmer lines and from metal lines. The median of the distribution of the error from Balmer lines is 78 G, from metal lines it is 130 G.

of similar SNR, the Balmer line analysis leads to results characterised by more homogeneous error bars than the metal line analysis.

7. Observations

In this survey we have observed 97 Ap stars, 138 normal A and B-type stars, and 22 non early-type stars. All these stars are candidate members of the open clusters (or the associations) listed in Table 2. Figure 6 gives an overview of the range in age and distance modulus of the target clusters, compared to all Milky Way open clusters with known age and $\delta \leq +10°$. A summary of the observing log is given in Table 3.

Target Ap stars have been selected as explained in Sect. 2.3, and are listed in Table A.1, together with the V magnitude and the spectral type extracted from the *General Catalogue of Ap and Am stars* (Renson et al. 1992), and from SIMBAD. Searching the literature (in particular the catalogue by

Table 2. List of open clusters observed in this survey, with approximate ages (Col. 4) and distance moduli $d = |M - m|$ (Col. 5) extracted from WEBDA. Column 6 gives the number of candidate peculiar stars and Col. 7 the number of non chemically peculiar A and B stars that we observed in each cluster.

RA & DEC	Name	log t	d	Ap	non Ap
00 04 07 −29 50 00	Blanco 1	7.796	7.18	1	0
04 48 27 +10 56 12	NGC 1662	8.625	9.14	1	0
05 26 +03 05	Ori OB1a ass.	7.07	7.6	2	0
05 36 −01 12	Ori OB1b ass.	6.23	8.37	4	0
05 35 −04 50	Ori OB1c ass.	6.66	8.52	8	3
05 27 −05 23	Ori OB1d ass.	6.0	8.52	2	1
06 08 24 +13 57 54	NGC 2169	7.067	10.73	1	4
06 28 01 −04 50 48	NGC 2232	7.727	7.87	1	0
06 31 55 +04 56 30	NGC 2244	6.896	12.23	1	3
06 46 01 −20 45 24	NGC 2287	8.385	9.29	3	2
06 54 12 −24 25 00	Collinder 121	7.054	8.45	1	0
07 02 42 −08 23 00	NGC 2323	8.096	10.50	1	2
07 08 06 −10 37 00	NGC 2343	7.104	10.48	0	28
07 15 20 −30 41 00	Collinder 132	7.080	8.48	1	0
07 36 35 −14 29 00	NGC 2422	7.861	8.67	4	2
07 43 12 −38 24 00	NGC 2451a	7.78	6.41	5	1
07 56 15 −30 03 48	NGC 2489	7.264	14.15	2	1
07 58 04 −60 45 12	NGC 2516	8.052	8.37	7	31
08 12 15 −37 35 42	NGC 2546	7.874	10.23	5	5
08 40 32 −53 02 00	IC 2391	7.661	6.24	2	0
08 47 54 −47 27 00	Trumpler 10	7.542	8.24	1	0
09 33 11 −53 23 54	NGC 2925	7.85	9.69	1	2
10 02 36 −60 07 12	NGC 3114	8.093	10.01	6	4
10 21 22 −54 21 22	NGC 3228	7.932	8.76	1	11
10 37 54 −59 11 00	vdb-Hagen 99	7.605	8.70	1	1
10 42 58 −64 24 00	IC 2602	7.507	6.11	1	0
10 42 04 −59 55 00	Collinder 228	6.830	12.77	2	2
11 05 39 −58 45 12	NGC 3532	8.492	8.55	3	3
14 07 27 −48 20 36	NGC 5460	8.207	9.44	3	2
14 35 37 −56 37 06	NGC 5662	7.968	10.08	2	5
16 18 50 −57 56 06	NGC 6087	7.976	10.29	2	3
16 35 47 −45 38 36	NGC 6178	7.248	10.71	2	0
16 41 20 −48 45 48	NGC 6193	6.775	11.79	2	2
17 04 41 −37 59 06	NGC 6281	8.497	8.86	2	1
17 34 48 −32 34 00	NGC 6383	6.962	10.89	2	6
17 40 20 −32 15 12	NGC 6405	7.974	8.88	4	9
17 53 51 −34 47 36	NGC 6475	8.475	7.71	3	0
18 27 15 +06 30 30	NGC 6633	8.629	8.44	2	0
18 31 47 −19 07 00	IC 4725	7.965	10.44	4	4
20 17 19 −79 02 00	Mel 227	8.57	5.52	1	0
TOTAL				97	138

Bychkov et al. 2003), we found that 10 of these Ap stars have already been checked for magnetic field in previous studies. We observed some of our objects more than once (we have made 121 observations of Ap stars). In total we obtained 52 field detections in 41 different stars (although for five stars we have only marginal detections). Thirty-seven Ap stars in which we have detected a field were not previously known as magnetic. A few Ap stars of Table A.1 are in fact *cluster non-members*. Chemical peculiarity, and, above all, cluster membership, will be further discussed in Paper II, where we will also provide estimates for star's temperature, mass, and evolutionary state. Two remarkable stars have been the subject of previous papers: HD 66318 (Bagnulo et al. 2003) and NGC 2244 338 (Bagnulo et al. 2004).

The normal A and B-type stars observed in this survey are listed in Table A.2, together with their V magnitudes and spectral classifications. In many cases the spectral type was not available in SIMBAD or in the literature, therefore, it has been determined through their color indices $B-V$ and $U-B$ extracted from WEBDA. The observed color indices have been corrected for extinction using the cluster $E(B-V)$ (also reported in WEBDA) and applying the extinction law by Cardelli et al. (1983). The dereddened colours have been then compared to those of typical main sequence stars to determine the approximate spectral type of each object. FORS1 spectra were used to roughly check the validity of this spectral classification, but no attempt was made to refine it. The spectral type obtained from the colour indices are reported between squared brackets, and should be used with caution. We discovered *a posteriori* that the spectra of ∼20 normal stars were in fact not of early-type. These cases are listed in Table A.5. We do not report observations of a few additional targets which have spectra with a too low SNR to be useful for magnetic studies.

In this work we report the $\langle B_z \rangle$ values obtained from the analysis of both Balmer lines and metal lines. For peculiar stars, the medians of the errors obtained from the Balmer lines and from the metal lines are 78 G, and 130 G, respectively. For normal stars they are 136 G, and 173 G, respectively. For normal stars the median error bar is larger than for peculiar stars because we optimized integration times to reach the highest possible SNR for Ap stars, rather than for the secondary targets added in the *fims mode* observations. In addition, we calculated the field measured from the analysis of the whole spectrum, including metal lines. The latter method formally gives $\langle B_z \rangle$ values with the smallest error bar: for Ap stars the median is 62 G, and for normal stars is 94 G. Although some caution is required in interpreting a $\langle B_z \rangle$ determination obtained combining Balmer and metal lines, one can reasonably argue that this method may be used to reinforce the conclusions achieved with the two primary methods.

The $\langle B_z \rangle$ determinations for Ap stars and for normal A and B stars are reported in Tables A.3 and A.4, respectively. These tables are organized as follows. The day and time of the observations are given in Cols. 2, and 3, respectively, and correspond to the midpoint between the instant when the shutter opens for the first exposure and the time when the shutter closes after the last exposure. Columns 4–6 report the $\langle B_z \rangle$ values obtained from the analysis of the Balmer lines, the metal lines, and the whole spectrum, respectively. All these $\langle B_z \rangle$ values are obtained through the least-squares technique applied to the averaged V/I calculated via Eq. (13). For each method, we also systematically calculated $\langle B_z \rangle'$ from Eq. (17). The cases in which both Eqs. (16) and (18) are satisfied are indicated in Col. 7 with symbol "D". The cases where only one of these equations is satisfied are flagged with symbol "d". If neither of Eqs. (16) or (18) is satisfied, we use the symbol "n". For example, in HD 62992, using the average spectrum obtained via Eq. (13), we have measured from Balmer lines $\langle B_z \rangle = -190 \pm 65$ G. This value (slightly less than a 3-σ detection) is reported in col. 4 of Table A.3. From the average of the $\langle B_z \rangle$ values obtained from the individual spectra we obtain $\langle B_z \rangle' = -186 \pm 54$ G (not reported in Table A.3). This is above a 3-σ detection, hence to this $\langle B_z \rangle$ determination we associate the symbol "d".

This procedure is repeated for each method used (Balmer lines, metal lines, full spectrum), so that to each $\langle B_z \rangle$ value, a three-term flag is associated. This three-terms flag is meant to help to evaluate the significance of each field detection. A "DDD" sequence clearly indicates a firm field detection, and "nnn" sequence indicates a null detection, whereas intermediate cases deserve further investigation and discussion. In general, a "DnD" or "Dnd" sequence may still represent field detection, if the lack of a detection from the analysis of the metal lines can be explained by a metal spectrum with low line density. This is for instance the case of HD 35008 of Table A.3, where Balmer line analysis gives $\langle B_z \rangle = -340 \pm 72$ G, and metal line analysis gives $\langle B_z \rangle = -273 \pm 293$ G. Here note that metal line analysis does not confirm the magnetic field detection, but is still consistent with the field measured via Balmer line analysis. This star's spectrum is not rich in metal lines, explaining the large error bar of $\langle B_z \rangle$ obtained through the metal

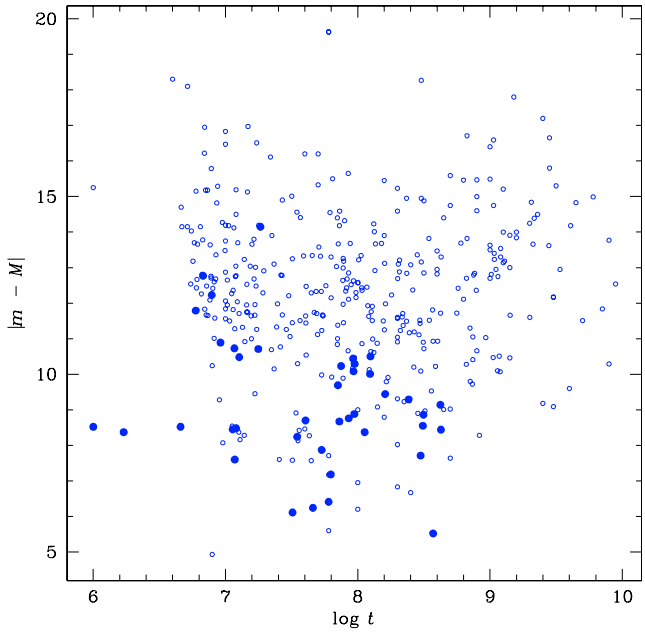

Fig. 6. Distance modulus versus age of open clusters. The empty circles show all open clusters with known age and $\delta < +10°$. Filled circles are the clusters observed in this survey (same data as in Table 2). Data have been extracted from WEBDA.

Table 3. Log of the various observing runs with FORS1 at the ESO VLT, dedicated to the open cluster survey.

Period	Program ID	Dates	Observing Mode	Telescope	Grism
P68	68.D-0403	2002 February 2/3 and 3/4	Visitor	UT3 Melipal	600 R
P70	70.D-0352	2003 February 7/8 and 8/9	Visitor	UT1 Antu	600 B & 600 R
P72	272.D-5026	2003 February 28/29 to March 2/3	Service	UT1 Antu	600 B
P73	73.D-0498	2004 May 28/29 to August 23/24	Service	UT1 Antu and UT2 Kueyen	600 B
P74	74.D-0488	2005 January 28/29 and 29/30	Visitor	UT2 Kueyen	600 B

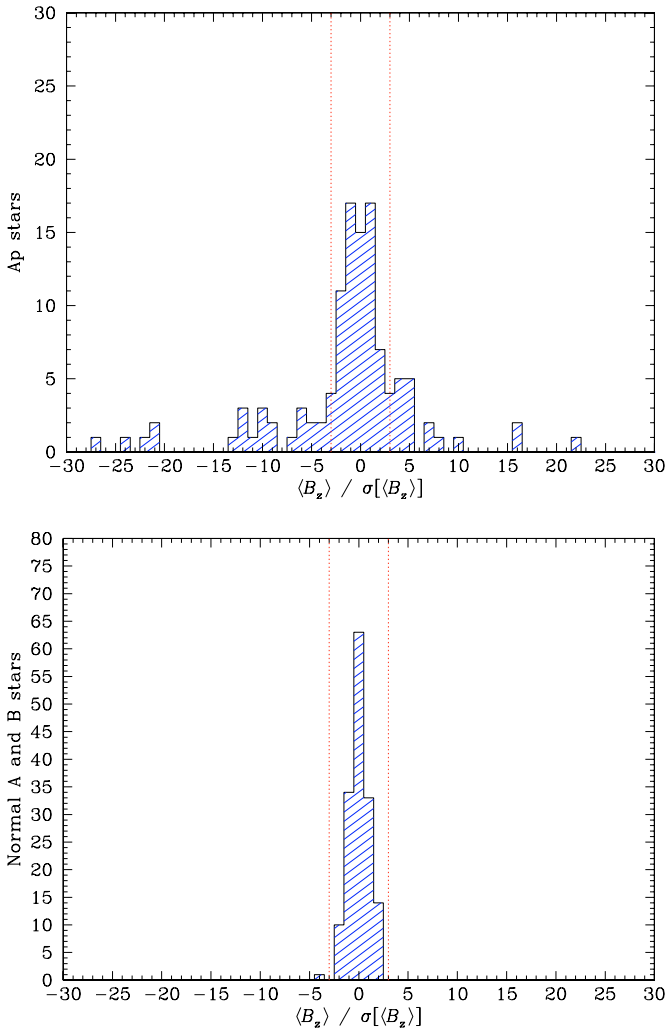

Fig. 7. Distribution of $\langle B_z \rangle$ values normalised to their error bars measured from Balmer lines in the Ap stars (upper panel) and in the normal A and B-type stars (lower panel). Five stars have been omitted from the upper panel (Ap stars) because they are off scale. The dotted lines correspond to the 3-σ detection level.

line method. By contrast, a "Dnn", or a "dnn" sequence in a star with a large blocking factor would prompt a re-analysis of the data reduction, or defer judgment about field detection to further observations.

8. Discussion

In Fig. 7 we show the histograms of the $\langle B_z \rangle$ values calculated via Balmer line analysis and normalized to their error bars. The upper panel refer to the Ap stars, and the lower panel refers to the normal early-type stars. The top histogram shows that in 58% of the observed Ap stars we obtained a null detection. However, it would be incorrect to infer that only ∼40% of the Ap stars are magnetic. First, targets of Table A.1 have not been carefully checked for correct spectral classification, and some may not be chemically peculiar. Secondly, and most importantly, our magnetic field detection threshold is usually ∼250 G, whereas observations based on high resolution spectropolarimetry have shown that a number of Ap stars exhibit a smaller longitudinal field (e.g., Aurière et al. 2004). Finally, some of our targets may have been observed at rotation phases at which the longitudinal field is small. This appears to be the case for HD 74169, for which we detected a field in only one of two measurements. More detailed statistical considerations will be presented in Paper II.

Conversely, the bottom histogram of Fig. 7 shows that no star among the normal A and B-type shows evidence for magnetic field to a typical 3 σ detection limit of 400 G. This is fully consistent with the null detections obtained by Landstreet (1982) and by Shorlin et al. (2002) in their surveys based on Hβ photopolarimetry, and high resolution spectropolarimetry of metal lines, respectively. Landstreet (1982) observed 31 targets (including normal A and B stars, Am, HgMn and λ Bootis stars) providing measurements with a median error of 65 G. Shorlin et al. (2002) observed 64 targets with a typical error between 15 and 50 G. Our survey has a larger detection threshold, but is based on a larger sample. Therefore, our results bring substantial additional support to the common belief that Ap stars are the only objects of the middle main sequence characterized by strong, globally organized, magnetic fields.

Statistical data about rotation velocities show that the typical $v_e \sin i$ values for normal A and B-type stars are in the range 100−200 km s^{-1}, depending on the stellar mass. It is therefore reasonable to assume that our targets have $v_e \sin i$ within the same range. Considering that observations based on high resolution spectropolarimetry are not suitable for field detection in rapidly rotating objects (say $v_e \sin i \gtrsim 60$ km s^{-1}), our work represents the most extensive survey for magnetic fields in normal early-type stars, and is not biased toward slowly rotating stars. The null result of this survey suggests that magnetic field organized on large scales are not common in non-Ap stars. Finally, and most important, the null detection obtained in non-Ap stars shows strong evidence that the diagnostic techniques used in this paper are not prone to spurious detections. The only exception is the star CD-60 1996, which deserves further investigation. Note however that with this many stars, statistically one should expect at least one measurement for which $|\langle B_z \rangle / \sigma[\langle B_z \rangle]| > 3$, even in absence of any magnetic fields.

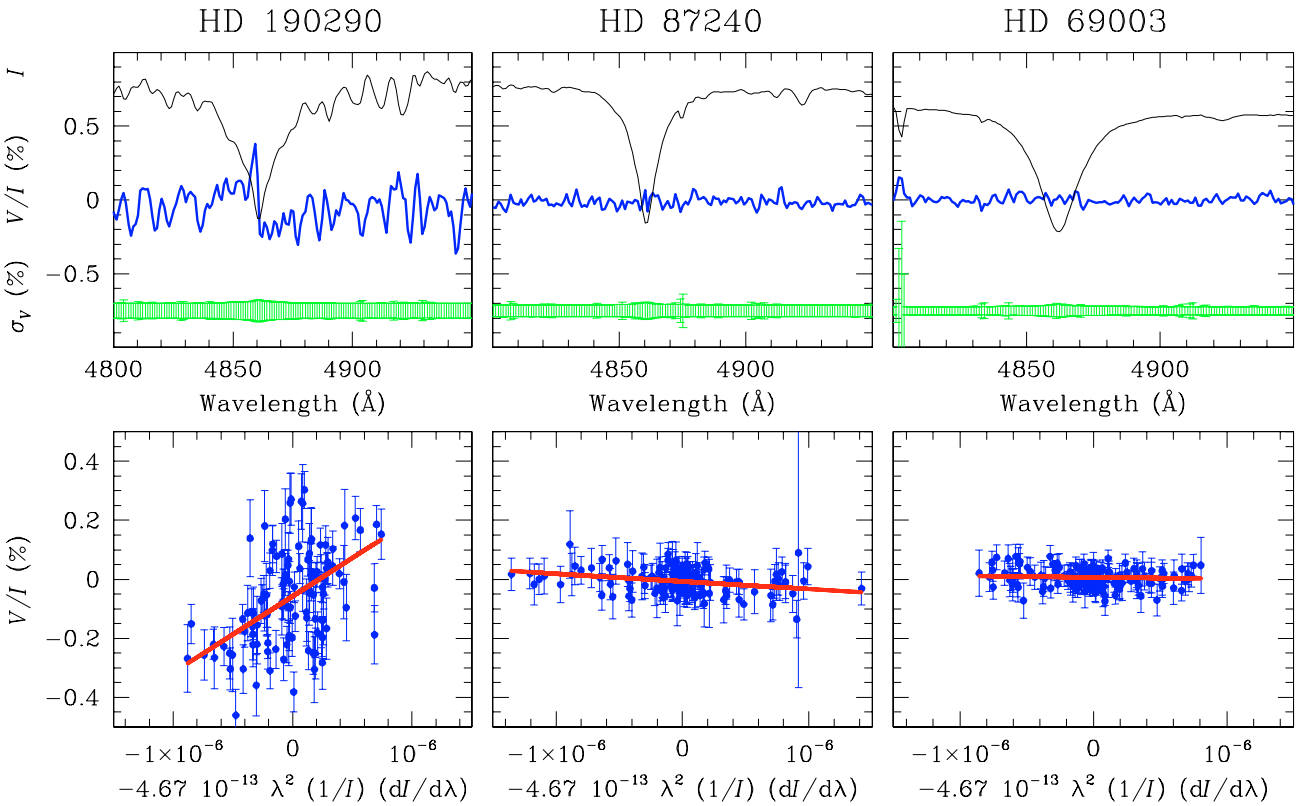

Fig. 8. Top panels: Stokes I (thin solid lines, arbitrary units) V/I profiles (thick solid line, in %), and error bar associated to V/I, for three stars observed during the survey. Bottom panels: the corresponding best-fit to the Balmer lines obtained by minimizing the χ^2 of Eq. (3). The longitudinal field measured in HD 190290 (left panels) is $\langle B_z \rangle = +2429 \pm 110$ G; the field measured in HD 87240 (middle panels) is -257 ± 58 G; the field measured in HD 69003 (right panels) is -48 ± 53 G.

Examples of reduced data and $\langle B_z \rangle$ determinations for three selected stars are illustrated in Fig. 8, which shows I and V/I around Hβ, as well as the best fit obtained applying Eq. (1) to all the Balmer lines. HD 190290 (left panels) exhibits a strong longitudinal field: $\langle B_z \rangle = +2429 \pm 110$ G. HD 87240 (middle panels) has a magnetic field close to the detection limit: $\langle B_z \rangle = -257 \pm 58$ G. HD 69003 (right panels) is a normal A-type star, and we did not detect a magnetic field ($\langle B_z \rangle = -48 \pm 53$ G). Note that a simple inspection to the V/I profile of HD 87240 (middle panels) does not show any obvious polarization signal. The magnetic field is detected by the linear correlation between V/I and the quantity $1/I \times \mathrm{d}I/\mathrm{d}\lambda$.

Table A.5 reports a field detection in the star HD 298045 which is of spectral type M3. Although a field detection in a M giant would be an exciting discovery, this result must be taken very cautiously. The spectrum of the star is contaminated by a strong reflection from the LADC (see Sect. 5.1), and, although we have measured $\langle B_z \rangle$ using only those spectral regions that appear not contaminated, it is clear that the validity of our measurement is highly questionable. In any case, it would be certainly interesting to extend our technique also to late type stars.

9. Conclusions

We have carried out a survey of magnetic fields in A- and B-type stars belonging to open clusters and associations. The mean longitudinal magnetic field $\langle B_z \rangle$ has been measured in 257 stars, via the analysis of their circularly polarized spectra obtained with the FORS1 instrument of the ESO VLT. The results of this survey will be used, in Paper II, to study how magnetic fields of early-type stars change as stars evolve through the main sequence phase.

For the benefit of other FORS1 observers, we have discussed in depth the technical details of our strategy for observations, data reduction and data analysis. In particular, we have shown that a combined analysis of metal and H Balmer lines represents in many cases the best strategy to detect a weak stellar magnetic field.

Among the observed targets, 97 are candidate Ap cluster member stars. A magnetic field was detected in 41 Ap stars, 37 of which were not previously known as magnetic stars. In none of the remaining 160 non-peculiar stars have we detected a field. Among these, 138 are presumably normal A and B type stars, and 22 are late-type stars. The fact that no field was detected in any of the stars that are traditionally considered non magnetic convincingly shows that the techniques used in this paper are not prone to spurious detections. At the same time, this work represents one of the largest surveys for magnetic fields in *normal* A and B-type stars. The precision of this survey is not as high as that obtained through high resolution spectropolarimetry, but our survey is *not* biased toward slowly rotating stars.

Before this work, only 13 candidate Ap cluster members, together with another 25 Ap stars belonging to the Ori B and Sco-Cen association, had been searched for a magnetic field. Our survey has obtained observations for an additional 90 Ap possible cluster members, and added about 30 more clusters to the list of those that have been searched for magnetic stars. For the first time we have now enough observational material to perform a preliminary search for links between magnetic field and evolution of Ap stars. This will be the subject of Paper II.

Acknowledgements. S.B., J.D.L., V.A., and G.A.W. are very grateful to W.W. Weiss for his kind hospitality at the Institut für Astronomie, Universität Wien. We wish to thank O. Kochukhov, F. Patat, and Th. Szeifert for useful discussions and suggestions. S.B. acknowledges DGDF 05/02 granted for a science leave in Wien. J.D.L. and G.A.W. acknowledge research support from the Natural Sciences and Engineering Research Council of Canada. JDL and VA acknowledge funding from the Scientific Visitors Programme of ESO Chile. This research has made use of the Simbad database, operated at CDS, Strasbourg, and of the WEBDA database, developed by J. Mermilliod and maintained at the Vienna Observatory by E. Paunzen.

References

Abt, H. A. 1979, ApJ, 230, 485
Aurière, M., Silvester, J., Wade, G. A., et al. 2004, in The A-star puzzle, ed. J. Zverko, J. Žižňovský, S. J. Adelman, & W. W. Weiss (Cambridge University Press), IAUS, 224, 633
Babcock, H. W. 1947, ApJ, 105, 105
Babcock, H. W. 1958, ApJS, 3, 141
Bagnulo, S., Szeifert, T., Wade, G. A., Landstreet, J. D., & Mathys, G. 2002, A&A, 389, 191
Bagnulo, S., Landstreet, J. D., Lo Curto, G., Szeifert, T., & Wade, G. A. 2003, A&A, 403, 645
Bagnulo, S., Hensberge, H., Landstreet, J. D., Szeifert, T., & Wade, G. A. 2004, A&A, 416, 1149
Bevington, P. R. 1969, Data reduction and error analysis for the physical sciences (New York: McGraw-Hill)
Bohlender, D. A., Landstreet, J. D., & Thompson, I. B. 1993, A&A, 269, 355
Bohlender, D. A., & Landstreet, J. D. 1990, MNRAS, 247, 606
Borra, E. F. 1981, ApJ, 249, L39
Borra, E. F., & Landstreet, J. D. 1975, PASP, 87, 961
Borra, E. F., & Landstreet, J. D. 1980, ApJS, 42, 421
Borra, E. F., Landstreet, J. D., & Thompson, I. 1983, ApJS, 53, 151
Bychkov, V. D., Bychkova, L. V., & Madej, J. 2003, A&A, 407, 631
Carrier, F., Burki, G., & Richard, C. 1999, A&A, 341, 469
Cardelli, J. A., Clayton, G. C., & Mathis, J. S. 1989, ApJ, 345, 245
Casini, R., & Landi Degl'Innocenti, E. 1994, A&A, 291, 668
Castellani, V., Chieffi, A., & Straniero, O. 1992, ApJS, 78, 517
Chen, L., Hou, J. L., & Wang, J. J. 2003, AJ, 125, 1397
Conti, P. S. 1970, ApJ, 159, 723
Cowley, C. R., & Bord, D. J. 2004, in The A-Star Puzzle, ed. J. Zverko, J. Žižňovský, S. J. Adelman, & W. W. Weiss (Cambridge University Press), IAUS, 224, 265
de Zeeuw, P. T., Hoogerwerf, R., de Bruijne, J. H. J., Brown, A. G. A., & Blaauw, A. 1999, ApJ, 117, 354
Dachs, J., & Kabus, H. 1989, A&AS, 78, 25
Dias, W. S., Lépine, J. R. D., & Alessi, B. S. 2001, A&A, 376, 441
Donati, J.-F., Semel, M., Carter, B. D., et al. 1997, MNRAS, 291, 658
Elkin, V. G., Kudryavtsev, D. O., & Romanyuk, I. I. 2003, AstL, 29, 400
Gomez, A. E., Luri, X., Grenier, S., et al. 1998, A&A, 336, 953
Joncas, G., & Borra, E. F. 1981, A&A, 94, 134
Hartoog, M. R. 1976, ApJ, 205, 807
Hartoog, M. R. 1977, ApJ, 212, 723
Hauck, B., & North, P. 1982, A&A, 114, 23
Hauck, B., & North, P. 1993, A&A, 269, 403
Høg, E., Kuzmin, A., Bastian, U., et al. 1998, A&A, 335, L65
Høg, E., Fabricius, C., Makarov, V. V., et al. 2000, A&A, 355, L27
Houk, N., & Smith-Moore, M. 1988, Michigan Spectral Survey, Ann Arbor, Dept. of Astronomy, Univ. of Michigan, Vol. 4
Huber, P. J. 1981, Robust Statistics, ed. J. Wiley, & Sons, New York
Hubrig, S., North, P., & Mathys, G. 2000, ApJ, 539, 352
Hubrig, S., Szeifert, T., Schöller, M., Mathys, G., & Kurtz, D. W. 2004, A&A, 415, 685
Kochukhov, O., & Bagnulo, S. 2006, A&A, in press [arXiv:astro-ph/0601461]
Kramer, N., & Maeder, A. 1980, A&A, 88, 135
Kupka, F., Paunzen, E., & Maitzen, H. M. 2003, MNRAS, 341, 849
Landstreet, J. D. 1982, ApJ, 258, 639
Landstreet, J. D., & Mathys, G. 2000, A&A, 359, 213
Lanz, T. 1984, A&A, 139, 161
Maitzen, H. M. 1993, A&AS, 102, 1
Mathys, G. 1991, A&AS, 89, 121
Mathys, G. 1994, A&AS, 108, 547
Mathys, G. 2004, in The A-Star Puzzle, ed. J. Zverko, J. Žižňovský, S. J. Adelman, & W. W. Weiss (Cambridge University Press), IAUS, 224, 225
Mathys, G., & Hubrig, S. 1997, A&AS, 124, 475
Mathys, G., Hubrig, S., Landstreet, J. D., Lanz, T., & Manfroid, J. 1997, A&AS, 123, 353
Mermilliod, J.-C., & Paunzen, E. 2003, A&A, 410, 511
Napiwotzki, R., Schönberner, D., & Wenske, V. 1993, A&A, 268, 653
Pöhnl, H., Paunzen, E., & Maitzen, H. M. 2005, A&A, 441, 1111
Preston, G.W., & Stępień, K. 1968, ApJ, 151, 577
Renson, P. 1992, Bull. Inf. Centre Donnees Stellaires, 40, 97
Renson, P., Gerbaldi, M., & Catalano, F. A. 1991, A&AS, 89, 429
Robichon, N., Arenou, F., Mermilliod, J.-C., & Turon, C. 1999, A&A, 345, 471
Ryabchikova, T., Wade, G. A., Aurière, M., et al. 2005, A&A, 429, 55
Sargent, W. L. W., Sargent, A. I., & Strittmatter, P. A. 1967, ApJ, 147, 1185
Schaerer, D., Meynet, G., Maeder, A., & Schaller, G. 1993, A&AS, 98, 523
Schaller, G., Schaerer, D., Meynet, G., & Maeder, A. 1992, A&ASS, 96, 269
Seifert, W., Appenzeller, I., Fürtig, W., et al. 2000, SPIE, 4008, 96
Shorlin, S. L. S., Wade, G. A., Donati, J.-F., et al. 2002, A&A, 392, 637
Sokolov, N. A. 1998, Contributions of the Astronomical Observatory Skalnate Pleso, 27, 261
Stępień, K. 2000, A&A, 353, 227
Stępień, K., & Dominiczak, R. 1989, A&A, 219, 197
Thompson, I. B., Brown, D. N., & Landstreet, J. D. 1987, ApJS, 64, 219
Wade, G. A., Donati, J.-F., Landstreet, J. D., & Shorlin, S. L. S. 2000, MNRAS, 313, 851

Online Material

Appendix A: The standard deviation of $\overline{V/I}$

We begin by defining, for brevity and clarity, the following quantities:

$$v \equiv \frac{V}{I}, \tag{A.1}$$

$$\phi^{\pm} \equiv \left(\frac{f^{\rm o} - f^{\rm e}}{f^{\rm o} + f^{\rm e}}\right)_{\alpha=\pm 45^\circ}. \tag{A.2}$$

With these definitions, Eq. (7) becomes:

$$v = \phi^- - \phi^+. \tag{A.3}$$

We now consider a sequence of n exposures taken with $\alpha = -45^\circ$, and m exposures taken with $\alpha = +45^\circ$, thus obtaining a set of $K = n\,m$ pairs, $v_{ij} = \phi_i^- - \phi_j^+$. In general we have that $m \neq n$, if for instance one or more data point have been rejected by the σ-clipping algorithm described in Sect. 5.3.

From such a set of measurements, we estimate the expected value for v using Eq. (13), that is:

$$\bar{v} \equiv \frac{\sum_{ij} v_{ij}/\sigma_{ij}^2}{\sum_{ij} 1/\sigma_{ij}^2}, \tag{A.4}$$

where we have shortened the notation for $\sigma^2[v_{ij}] = \sigma^2[\phi_i^-] + \sigma^2[\phi_j^+]$ with σ_{ij}^2.

We now wish to estimate the variance of the statistical variable $\bar{v}$:

$$\sigma^2[\bar{v}] = \left\langle (\bar{v} - \langle v\rangle)^2 \right\rangle = \left(\sum_{i=1}^{n}\sum_{j=1}^{m} \sigma_{ij}^{-2}\right)^{-2} \times \left(\sum_{i,h=1}^{n}\sum_{j,k=1}^{m} \sigma_{ij}^{-2}\sigma_{hk}^{-2} \left\langle (\phi_i^- - \phi_j^+ - \langle v\rangle)(\phi_h^- - \phi_k^+ - \langle v\rangle)\right\rangle\right),$$

where $\langle v\rangle$ is of course the mean value of v and of $\bar{v}$. Since, obviously, $\langle v\rangle = \langle\phi^-\rangle - \langle\phi^+\rangle$ (from Eq. (A.3)), and since the various exposures are statistically uncorrelated (thus the covariance $\sigma[\phi^-, \phi^+] = 0$), it is easy to derive:

$$\sigma^2[\bar{v}] = \left(\sum_{i=1}^{n}\sum_{j=1}^{m} \sigma_{ij}^{-2}\right)^{-2} \times \left[\sum_{i=1}^{n}\sum_{j=1}^{m} \sigma_{ij}^{-2}\left(\sigma^2[\phi_i^-]\sum_{k=1}^{m}\sigma_{ik}^{-2} + \sigma^2[\phi_j^+]\sum_{h=1}^{n}\sigma_{hj}^{-2}\right)\right]. \tag{A.5}$$

If all errors of individual exposures can be assumed equal:

$$\sigma^2[\phi_i^-] = \sigma^2[\phi_j^+] = \sigma_{ij}^2/2 = \sigma^2/2, \tag{A.6}$$

for $i = 1, \ldots n$ and $j = 1, \ldots m$, Eqs. (A.4) and (A.5) become, respectively:

$$\bar{v} = \frac{1}{n\,m}\sum_{ij} v_{ij} = \overline{\phi^-} - \overline{\phi^+} \tag{A.7}$$

$$\sigma^2[\bar{v}] = \frac{\sigma^2}{2}\left(\frac{1}{n} + \frac{1}{m}\right). \tag{A.8}$$

The latter equation, in particular, reduces to Eq. (14) if $n = m$. In this case, it is worth noting that at the denominator of Eq. (14) there appears m instead of the number of exposure pairs $K = m^2$, as it would naively be expected from the analogy with the average of m^2 independent measures. The reason is obviously that the m^2 combinations are not all completely independent from each other, since each exposure is counted m times in Eqs. (13) and (A.4).

It would be desirable to find an alternative to Eq. (A.5) that does not depend explicitly on the knowledge of the statistical errors of the individual exposures. We seek an estimator of the form:

$$s^2 = C\,\sum_{ij}\left(v_{ij} - \bar{v}\right)^2,$$

where C is a constant such that the statistical estimator s^2 is not biased, i. e. its mean value coincides with the expected value $\sigma^2[\bar{v}]$. We find such a constant under the assumption that all errors of individual exposures are assumed equal (Eq. A.6):

$$\begin{aligned}\left\langle s^2\right\rangle &= C\,\left\langle\sum_{ij}\left(v_{ij} - \bar{v}\right)^2\right\rangle \\ &= C\,\sum_{ij}\left\langle\left[(v_{ij} - \langle v\rangle) - (\bar{v} - \langle v\rangle)\right]^2\right\rangle \\ &= C\,\left[n\,m\left(\sigma^2[v] + \sigma^2[\bar{v}]\right) - 2n\,m\,\left\langle(\bar{v} - \langle v\rangle)^2\right\rangle\right] \\ &= C\,\left[n\,m\left(\sigma^2[v] - \sigma^2[\bar{v}]\right)\right] \\ &= C\,\left[m\,(n-1) + n\,(m-1)\right]\sigma^2/2,\end{aligned}$$

where in the last passage we have used Eq. (A.8). From the above expressions, the estimator s^2 is unbiased if it is defined as:

$$s^2 = \frac{1}{m\,n\,[2\,n\,m/(n+m) - 1]}\,\sum_{ij}\left(v_{ij} - \bar{v}\right)^2, \tag{A.9}$$

which, of course, becomes Eq. (15) if $m = n$.

Table A.1. List of Ap star candidate open cluster members. Magnitude and spectral types are taken from the *General catalogue of Ap and Am stars* by Renson et al. (1992), and/or from SIMBAD. In Col. 6 we report a flag about peculiarity confidence from the same catalogue. Symbol * means "well knonw Ap star", symbol "?" means "doubtful nature"; we indicate with "–" the cases in which the star is not included in the Renson et al's catalogue (in which case spectral type is taken from SIMBAD or specific literature). The star's actual membership and peculiarity will be discussed in Paper II.

Cluster	ID1	ID2	V	Spectral Type	CP prob.
Blanco 1	HD 225264	CD-30 19818	8.3	A1 Si Sr	?
NGC 1966	HD 30598	BD+10 649	9.1	A1 Sr Cr	
Ori OB1 Ass.	HD 35008	BD-01 872	7.1	B9 Si	?
	HD 36046	BD-00 964	8.1	B8 He-weak	
	HD 36540	BD-04 1162	8.1	B7 He-weak	
	HD 36549	BD+01 1053	8.6	B7 He-weak	
	HD 36629	BD-04 1164	7.7	B3 He-weak	?
	HD 36918	BD-06 1231	8.3	B9 He-weak	?
	HD 36916	V1045 Ori	6.7	B8 He-weak Si	*
	HD 36960	BD-06 1234	4.8	B0 Si	
	HD 36982	VM LP Ori	8.4	B2 He	?
	HD 290665	BD-00 1008	9.4	A0 Cr Eu Sr	
	HD 37022	tet01 Ori C	5.1	O6pe	–
	HD 37058	V359 Ori	7.3	B3 He-weak Sr	*
	HD 37210	V1133 Ori	8.1	B8 He-weak Si	
	HD 37333	BD-02 1319	8.5	A0	?
	HD 37470	BD-06 1274	8.2	B8 Si	
	HD 37633	V1147 Ori	9.0	B9 Si Eu	
NGC 2169	V1356 Ori	NGC 2169 12	10.8	A0 Si	
NGC 2232	HD 45583	V682 Mon	8.0	B9 Si	
NGC 2244	NGC 2244 334	GSC 00154-02164	12.9	B3	–
NGC 2287	HD 49023	BD-20 1543	8.4	B9 Hg Si	
	CPD-20 1640	NGC 2287 AR 143	11.1	A5 Si Sr	–
	HD 49299	BD-20 1573	10.2	A0 Si Sr Cr	
Collinder 121	HD 51088	CD-24 4586	8.3	B8 Si	?
NGC 2323	HD 52965	BD-08 1701	9.2	B8 Si	?
Collinder 132	HD 56343	CD-31 4243	9.2	B9	–
NGC 2422	BD-14 2015	NGC 2422 70	9.5	B9 Sr	
	BD-14 2028	NGC 2422 88	10.4	A1 Sr Cr	?
	HD 61045	BD-14 2029	8.0	B8 Si	
	BD-14 2040	NGC 2422 103	10.6	A1 Sr Cr	?
NGC 2451	HD 62376	CD-38 3564	6.5	B7	–
	CD-37 3845	NGC 2451 36	8.6	A0 Si	?
	HD 62992	CD-37 3860	7.9	A4 Sr Eu	
	HD 63079	CD-37 3868	7.0	B9 Si	?
	HD 63401	OX Pup	6.3	B9 Si	
NGC 2489	NGC 2489 58	NGC 2489 PM 39	12.8	A0	–
	NGC 2489 40	NGC 2489 PM 54	12.6	B5	–
NGC 2516	HD 65712	CD-60 1925	9.4	A0 Si Cr	
	CPD-60944A	NGC 2516 DAC 73	8.3	B9 Si	
	CPD-60944B	NGC 2516 DAC 74	8.8	B9 Si	?
	CPD-60 978	V 391 Car	8.9	A0 Si Cr Eu	
	HD 65987	V356 Car	7.6	B9 Si Sr	*
	HD 66295	V422 Car	9.1	B9 Si	
	HD 66318	NGC 2516 DAC 95	9.6	A0 Eu Cr Sr	*
NGC 2546	NGC 2546 258	–	10.6	–	–
	NGC 2546 201	–	?	–	–
	CPD-37 1989	NGC 2546 197	11.0	A2	?
	HD 69004	CD-37 4414	9.4	B8 Si	?

Table A.1. continued.

Cluster	ID1	ID2	V	Spectral Type	CP prob.
	HD 69067	CD-37 4420	8.3	B8 Si	
IC 2391	HD 74169	KR Vel	7.2	A1 Si Cr Sr	*
	HD 74535	KT Vel	5.6	B9 Si	*
Trumpler 10	HD 75239	CD-41 4498	9.2	B9 Si	
NGC 2925	HD 83002	CD-52 3172	9.1	B8 Si	
NGC 3114	HD 87241	CD-59 2746	7.8	B9 Si	?
	HD 87240	CPD-59 1673	9.6	B9 Si	
	HD 87266	CD-59 2755	8.2	B3 Si N	
	HD 304841	CPD-59 1717	10.0	A	?
	HD 304842	V424 Car	9.7	B8 Si	
	HD 87405	CD-59 2803	8.5	B9 Si	
NGC 3228	HD 89856	CD-51 4685	9.1	B8	?
vdB-Hagen88	HD 92190	CD-58 3407	8.6	B8	–
IC 2602	HD 92385	V 407 Car	6.7	B9 Si	
Collinder 228	Collinder 228 30	Collinder 228 CP4	10.8	B1	–
	HD 305451	CPD-59 2496	10.5	B9 Si	?
NGC 3532	HD 96040	CPD-57 4168	10.7	A	?
	HD 96729	CPD-58 3157	10.0	B9 Si	
	HD 303821	NGC 3532 241	11.7	A	?
NGC 5460	HD 122983	CD-47 8870	9.9	A0	?
	HD 123183	CD-47 8895	9.9	A0	–
	HD 123225	CD-47 8901	8.9	B9 Si	?
NGC 5662	CPD-56 6330	NGC 5662 85	10.6	A2	
	HD 127866	CD-56 5516	8.3	B8	–
NGC 6087	CPD-57 7817	NGC 6087 25	10.0	–	?
	HD 146555	CPD-57 7872	10.3	B9 Si	
NGC 6178	HD 149257	CD-45 10768	8.5	B5 He	
	HD 149277	CD-45 10769	8.4	B2	–
NGC 6193	CD-48 11051	CPD-48 8684	10.4	B1	–
	CD-48 11059	NGC 6193 VF 33	10.7	B3	–
NGC 6281	HD 322676	CD-37 11203	10.2	A0	–
	HD 153948	V948 Sco	9.3	A2 Si	
NGC 6383	NGC 6383 26	NGC 6383 FJL 5	12.9	A	–
	HD 317857	NGC 6383 3	10.3	A2	–
NGC 6405	HD 318107	V970 Sco	9.3	B8	?
	HD 318100	V971 Sco	9.8	B9	
	CD-32 13119	NGC 6405 7	10.9	–	?
	HD 318095	–	10.9	A0	?
NGC 6475	HD 162305	CD-34 12154	7.8	B9	?
	HD 320764	CD-34 12161	8.9	A6	?
	HD 162725	V951 Sco	6.4	B9 Si Cr	*
NGC 6633	HD 169959	BD+06 3762	7.8	A0 Si	
	HD 170054	BD+06 3772	8.2	B7 Si	
IC 4725	BD-19 5044L	CPD-19 6897	10.2	B8	?
	BD-19 5046	CPD-19 6905	9.0	A1	–
	HD 170836	BD-19 5052	9.0	B7	?
	HD 170860A	BD-19 5058	9.4	B8	–
Melotte 227	HD 190290	CK Oct	9.9	A0 Eu Sr	

Table A.2. List of the observed normal cluster A and B-type stars. Actual membership has not been checked. Spectral types reported between square brackets were estimated from the star's colour indices, and should be taken with caution.

Cluster	ID1	ID2	V	Spectral Type
Ori OB1 Ass.	HD 36559	BD-04 1163	8.8	B9
	HD 36671	BD-04 1165	8.7	B9
	HD 37041	tet02 Ori A	5.1	O9.5Vpe
	HD 37428	BD-06 1271	8.8	A0
NGC 2169	HD 252214	BD+13 1120	8.1	B2.5V
	HD 41909	BD+14 1160	8.4	B5
	HD 252248	BD+13 1123	8.8	B2V
	HD 252266	BD+13 1124E	9.2	B3V
NGC 2244	NGC 2244 336	GSC 00154-01288	12.6	A0
	CPD-20 1637	NGC 2287 54	10.9	A1V
	BD-20 1571	NGC 2287 55	10.8	A3
NGC 2287	NGC 2287 AR 157	–	?	?
	CPD-20 1645	NGC 2287 AR 159	?	?
NGC 2323	HD 52980	BD-08 1796	8.4	B9
	BD-08 1708	NGC 2323 51	9.9	B6
NGC 2343	CSI-10-07049	NGC 2343 13	10.9	–
	BD-10 1875	NGC 2343 9	10.6	[A0]
	NGC 2343 22	CSI-10-07051	11.8	[A0V]
	NGC 2343 40	CSI-10-07053 3	13.1	[F1?V]
	CSI-10-07053 5	NGC 2343 35	12.9	[A6V]
	BD-10 1878	NGC 2343 12	10.8	[B8/9]
	NGC 2343 25	CSI-10-07054 1	11.7	[A3/4V]
	NGC 2343 16	CSI-10-07055 1	11.4	[A8?]
	BD-10 1879a	NGC 2343 7	10.3	[A3V]
	NGC 2343 34	CSI-10-07056 5	12.7	[A6V]
	NGC 2343 43	CSI-10-07056 6	13.6	[F?]
	NGC 2343 28	CSI-10-07055 2	12.5	[A5V]
	NGC 2343 37	CSI-10-07055 3	13.1	[A8?]
	HD 54304	BD-10 1882	9.9	A
	NGC 2343 27	CSI-10-07056 4	12.4	[A5/6V]
	NGC 2343 26	CSI-10-07057 4	12.3	[A7]
	NGC 2343 6	CSI-10-07057 1	10.3	[B8?]
	NGC 2343 36	CSI-10-07058 8	13.0	[A7/8?]
	NGC 2343 17	CSI-10-07057 3	11.7	[A2/3V]
	NGC 2343 10	CSI-10-07057 2	10.5	[B8/9?]
	NGC 2343 31	CSI-10-07058 7	12.6	[A6]
	BD-10 1883B	–		
	BD-10 1883A	NGC 2343 5	10.1	[B9]
	NGC 2343 18	CSI-10-07058 1	11.4	[A4V]
	NGC 2343 38	CSI-10-07058 6	13.0	[A7/8]
	HD 54360	BD-10 1884	9.4	A0
	BD-10 1885B	NGC 2343 11	10.7	B9/A0?
	HD 54388	BD-10 1887	8.4	A3
NGC 2422	HD 60940	BD-14 2012	8.7	B7/B8III
	HD 60996	BD-14 2019	8.7	BV
NGC 2451	HD 62974	CD-37 3855	8.3	A3V
NGC 2489	NGC 2489 59	GSC 07119-01134	12.9	B9
NGC 2516	HD 65691	NGC 2516 DAC 9	9.0	B8/B9V
	CPD-60 942	NGC 2516 DAC 10	10.1	A1V
	CD-60 1929	NGC 2516 DAC 12	8.5	B9III
	CD-60 1932	NGC 2516 DAC 14	9.9	A0V
	HD 65869	CD-60 1937	7.7	B9V
	HD 65896	NGC 2516 DAC 18	9.4	A0V
	HD 65950	NGC 2516 DAC 27	6.9	B8III

Table A.2. continued.

Cluster	ID1	ID2	V	Spectral Type
	V373 Car	NGC 2516 DAC 28	9.0	B
	HD 65949	NGC 2516 DAC 26	8.4	B8/B9
	BD-60 969	NGC 2516 DAC 29	8.6	B9.5IV
	BD-60 975	NGC 2516 DAC 504	8.9	Avar
	CPD-60 977	NGC 2516 DAC 211	10.4	F0V
	V410 Car	NGC 2516 DAC 81	10.7	A7V
	V392 Car	NGC 2516 DAC 37	9.5	A2V
	CD-60 1967	NGC 2516 DAC 38	7.2	B9.5IV
	CD-60 1971	NGC 2516 DAC 42	8.1	B8.5V
	V417 Car	NGC 2516 DAC 40	10.4	[A6V]
	CPD-60 984	NGC 2516 DAC 41	9.7	A2V
	CPD-60 986	NGC 2516 DAC 901	10.1	[A2V]
	V418 Car	NGC 2516 DAC 43	11.0	[A6/7V]
	CD-60 1974	NGC 2516 DAC 607	9.4	A1V
	CD-60 1975	NGC 2516 SBL 753	8.4	B9V
	CD-60 1976	NGC 2516 DAC 48	9.7	A0V
	CD-60 1979	NGC 2516 DAC 615	10.8	A3V
	CD-60 1978	NGC 2516 DAC 49	8.8	B8.5IV-V
	CD-60 1981	NGC 2516 DAC 608	10.7	A1Vm
	V420 Car	NGC 2516 DAC 51	10.4	A3V
	HD 66137	NGC 2516 DAC 53	7.8	B9V:
	HD 66194	V374 Car	5.8	B2IVnpe
	CD-60 1996	NGC 2516 DAC 806	10.8	A8V
	CD-60 1999	NGC 2516 DAC 60	10.0	A2V
NGC 2546	[N75] 195	GSC 07133-00458	10.5	B3:
	[N75] 196	–	10.7	B3:
	NGC 2546 272	GEN #2.25460272	10.7	B3
	CD-37 4353	CPD-37 1983	?	?
	HD 69003	CD-37 4413	8.8	A0
NGC 2925	HD 298537	CPD-52 2517	11.0	A
	HD 298536	CPD-52 2522	–	AO
NGC 3114	NGC 3114 233	–	–	–
	CPD-59 1698	NGC 3114 54	10.8	–
	CPD-59 1700	NGC 3114 56	11.1	–
	CPD-59 1703	NGC 3114 65	11.0	–
NGC 3228	HD 298051	CD-51 4686	10.2	A1V
	HD 89901	V343 Vel	8.4	B8/B9III
	HD 89900	CD-51 4691	8.2	A0/A1IV/V
	HD 89915	CD-51 4693	7.8	B9.5V
	HD 89922	CD-51 4696	9.3	A4IV/V
	HD 298047	CD-51 4695	9.2	B9V
	HD 89938	CD-51 4698	9.3	A
	HD 89937	CD-51 4699	8.9	B6/B7
	HD 89956	CD-51 4701	8.2	B9IV/V
	CPD-51 3249	NGC 3228 15	11.3	[A8V]
	HD 298053	CD-51 4702	10.6	A3m
vdB-Hagen 88	HD 303107	HD 92234	9.6	B9
Collinder 228	HD 305535	Collinder 228 25	9.4	B2.5Vn
	HD 305543	DW Car	10.0	B5Iab
NGC 3532	HD 96653	CD-58 3835	8.4	A0III
	NGC 3532 447	–	9.7	[A5]
	HD 96790	CD-57 3718	10.1	B
NGC 5460	CD-47 8868	NGC 5460 36	10.7	A0
	HD 123201B	CD-47 8899B	9.1	A0
NGC 5662	HD 127835	CD-55 5723	9.4	B8V

Table A.2. continued.

Cluster	ID1	ID2	*V*	Spectral Type
	CPD-56 6334	NGC 5662 104	9.9	B9V
	NGC 5662 126	CPD-56 6337	10.7	A1V
	HD 127900	CD-55 5726	8.8	B8II/III
	HD 127924	CD-55 5727	9.2	B8III/IV
NGC 6087	NGC 6087 129	GEN# +2.60870129	11.5	–
	TYC 8719- 717-1	GSC 08719-00717	10.2	[A0]
	HD 146484	CPC 20 5173	9.5	A0
NGC 6193	CD-48 11050	CPD-48 8680	10.3	A2
	CD-48 11060	CPD-48 8694	10.7	B3V
NGC 6281	HD 323673	CD-37 11212	10.2	A5
NGC 6383	NGC 6383 28	GEN# +2.63830028	12.5	A
	NGC 6383 700	GEN# +2.63830700	12.7	–
	NGC 6383 87	–	13.7	–
	HD 317846	CPD-32 4611	9.9	B5
	NGC 6383 102	GEN# +2.63830102	14.6	–
	HD 317852	NGC 6383 21	11.9	A0
NGC 6405	HD 318108	CD-32 13080	9.7	B9
	HD 318109	–	9.9	A0
	CD-32 13089	NGC 6405 53	9.9	[A4]
	CD-32 13093	NGC 6405 52	10.2	[A0]
	V976 Sco	NGC 6405 31	11.5	[A?]
	HD 318099	CD-32 13111	9.9	A0
	HD 320765	CD-34 12156	8.8	A2
	HD 162678	CD-34 12219	6.4	B9V
	HD 162724	V906 Sco	6.0	B9V+
IC 4725	BD-19 5044 F	?	9.7	B8V
	BD-19 5045 ?	CPD-19 6899	9.1	B5
	BD-19 5044 M	CPD-19 6901	10.2	B8V
	HD 170835	BD-19 5055	8.8	B5IV

Table A.3. $\langle B_z \rangle$ measurements for chemically peculiar stars. Columns 2 and 3 give the date and UT at mid-exposure of the observation, respectively. Columns 4–6 report the $\langle B_z \rangle$ measurement from the Balmer lines, the metal lines, and the full spectrum, as explained in the text. Column 7 reports the flag for the $\langle B_z \rangle$ detection obtained from Balmer, metal lines, and full spectrum. The meaning of "D", "d", and "n" is explained in the text, in Sect. 7. Column 8 reports the signal to noise ratio (SNR) per Å calculated, for stars observed with grism 600 B, in the wavelength interval 4975–5025 Å (close to the red wing of Hβ). For stars observed with grism 600 R, the SNR was calculated in the wavelength interval 6640–6690 Å (i.e., close to the red wing of Hα). Column 9 is used to report flags and notes. Unless otherwise marked, the star was observed with grism 600 B.

ID1	Date	UT	$\langle B_z \rangle$ (G) Balmer lines	$\langle B_z \rangle$ (G) metal lines	$\langle B_z \rangle$ (G) full spectrum	Flag	SNR	Note
HD 225264	2004-07-31	09:49:40	-48 ± 38	71 ± 72	-23 ± 32	nnn	3900	
HD 30598	2004-09-01	07:42:15	124 ± 120	-55 ± 143	49 ± 90	nnn	1600	
	2005-01-29	01:54:58	121 ± 65	89 ± 94	118 ± 52	nnd	2500	
HD 35008	2005-01-29	00:22:02	-340 ± 72	-273 ± 293	-339 ± 69	DnD	2200	1, M (new)
HD 36046	2005-01-30	01:21:07	-27 ± 83	-110 ± 175	-39 ± 74	nnn	2000	
HD 36540	2003-02-08	01:40:07	301 ± 67	187 ± 115	277 ± 56	dnD	2700	1, M (new)
HD 36549	2005-01-30	02:01:45	-57 ± 80	-206 ± 223	-57 ± 74	nnn	1800	
HD 36629	2003-02-08	02:08:23	87 ± 66	-58 ± 73	15 ± 52	nnn	2600	2
HD 36918	2003-02-09	02:10:05	-13 ± 58	31 ± 150	6 ± 54	nnn	2700	
HD 36916	2003-02-09	01:00:16	-539 ± 56	-261 ± 123	-488 ± 51	DnD	2700	3,
HD 36960	2003-02-09	01:42:20	-90 ± 63	-132 ± 64	-115 ± 45	nnn	2900	
HD 36982	2003-02-08	01:11:00	238 ± 239	-192 ± 271	91 ± 193	nnn	750	
HD 290665	2005-01-29	01:20:42	-1778 ± 67	-1588 ± 64	-1664 ± 44	DDD	2250	M (new)
HD 37022	2003-02-08	01:11:00	57 ± 82	115 ± 82	86 ± 49	nnn	4150	
HD 37058	2003-02-09	00:41:09	-975 ± 77	-664 ± 87	-812 ± 59	DDD	2100	4, M
HD 37210	2003-02-09	01:21:46	29 ± 66	-157 ± 117	-30 ± 57	nnn	2250	1
HD 37333	2005-01-29	00:44:54	23 ± 63	-261 ± 117	-46 ± 55	nnn	2600	
HD 37470	2003-02-08	02:49:06	-62 ± 66	-185 ± 166	-62 ± 60	nnn	2450	1
HD 37633	2005-01-30	01:41:35	295 ± 83	292 ± 97	283 ± 62	DdD	2000	M (new)
V1356 Ori	2003-02-08	03:40:54	-3408 ± 144	-1290 ± 180	-2449 ± 113	DDD	1250	M (new)
HD 45583	2003-09-09	05:40:42	-1518 ± 71	-1370 ± 58	-1433 ± 44	DDD	2500	M (new)
NGC 2244 334	2003-02-09	03:52:60	-9515 ± 196	-4815 ± 136	-6215 ± 112	DDD	1100	5, M (new)
HD 49023	2005-01-30	02:21:14	79 ± 70	-48 ± 244	100 ± 68	nnn	2000	
CPD-20 1640	2005-01-30	03:35:37	204 ± 92	40 ± 101	157 ± 63	dnn	1850	
HD 49299	2004-09-28	08:26:26	-483 ± 42	-508 ± 37	-659 ± 83	DDD	3300	M (new)
	2005-01-30	02:50:57	-2720 ± 60	-2311 ± 77	-2598 ± 45	DDD	2200	M
HD 51088	2004-09-21	09:13:05	-118 ± 51	103 ± 103	-76 ± 45	nnn	2900	
	2005-01-30	05:22:22	-5 ± 74	384 ± 135	102 ± 64	ndd	1900	
HD 52965	2005-01-30	05:03:48	-69 ± 92	-105 ± 217	-64 ± 84	nnn	1800	
HD 56343	2004-09-21	08:32:57	-3609 ± 69	-3144 ± 90	-3415 ± 54	DDD	1950	M (new)
BD-14 2015	2005-01-29	05:47:41	-31 ± 72	-290 ± 258	-32 ± 69	nnn	2400	
BD-14 2028	2004-02-28	04:16:33	103 ± 112	-271 ± 218	32 ± 93	nnn	1550	
	2004-03-08	04:45:24	119 ± 130	-394 ± 240	-7 ± 104	nnn	1400	
HD 61045	2003-02-08	04:28:15	412 ± 63	476 ± 108	506 ± 111	Ddd	2500	M (new)
	2005-01-29	06:11:00	375 ± 70	186 ± 137	340 ± 62	DnD	2300	M
BD-14 2040	2003-02-08	04:28:15	169 ± 273	-149 ± 244	16 ± 166	nnn	750	
	2005-01-29	05:04:50	56 ± 72	-104 ± 101	-37 ± 55	nnn	2300	
HD 62376	2005-01-29	02:41:28	101 ± 62	-4 ± 127	73 ± 55	nnn	2450	
CD-37 3845	2003-02-08	04:52:12	98 ± 113	-430 ± 201	10 ± 97	ndn	1450	
HD 62992	2003-02-08	04:52:12	-190 ± 65	-157 ± 54	-164 ± 39	ddd	2450	M (new)
HD 63079	2005-01-29	02:21:48	8 ± 64	150 ± 152	47 ± 58	nnn	2300	
HD 63401	2003-02-08	00:36:57	-532 ± 61	-551 ± 119	-527 ± 53	DDD	2900	6, M (new)
	2005-01-29	02:59:47	357 ± 96	472 ± 195	348 ± 85	Dnd	2450	M
NGC 2489 58	2005-01-30	06:10:58	-325 ± 205	-826 ± 313	-449 ± 170	nnn	1200	
NGC 2489 40	2005-01-30	06:10:58	-489 ± 220	36 ± 251	-387 ± 158	nnn	850	
HD 65712	2003-02-09	07:20:21	-1025 ± 84	-1181 ± 73	-1111 ± 54	DDD	1800	M (new)
	2005-01-29	04:22:56	-668 ± 55	-357 ± 74	-558 ± 43	DDD	2450	M
CPD-60944A	2002-02-05	06:03:02	-41 ± 104	122 ± 87	48 ± 67	nnn	1950	7, R
	2005-01-29	03:25:09	-54 ± 58	-74 ± 113	-50 ± 51	nnn	2500	7
CPD-60944B	2002-02-05	06:55:01	274 ± 111	349 ± 67	349 ± 66	nDD	1450	7, R, m (new?)
	2005-01-29	03:52:30	143 ± 63	93 ± 89	158 ± 50	nnd	2650	7
CPD-60 978	2002-02-04	06:08:09	48 ± 103	-35 ± 71	2 ± 58	nnn	1750	R

Table A.3. continued.

ID1	Date	UT	$\langle B_z \rangle$ (G) Balmer lines	$\langle B_z \rangle$ (G) metal lines	$\langle B_z \rangle$ (G) full spectrum	Flag	SNR	Note
	2002-02-05	04:19:29	58 ± 83	39 ± 71	46 ± 54	nnn	1850	R
	2004-03-08	05:25:21	-91 ± 103	-229 ± 189	-83 ± 88	nnn	1650	
HD 65987	2002-02-04	07:54:30	629 ± 162	573 ± 142	605 ± 106	DDD	1400	R, M (new)
	2004-02-28	05:13:09	-443 ± 70	-507 ± 105	-460 ± 58	DDD	2150	M
HD 66295	2002-02-05	05:08:50	-547 ± 84	-515 ± 70	-534 ± 54	DDD	2000	R, M (new)
	2003-02-09	06:30:09	499 ± 73	421 ± 46	438 ± 38	DDD	2350	R, M
HD 66318	2002-02-05	05:08:50	4410 ± 105	5129 ± 40	5044 ± 37	DDD	1600	8, R, M (new)
	2003-02-09	06:30:09	4266 ± 85	5322 ± 31	5196 ± 29	DDD	1850	R, M
NGC 2546 258	2004-09-27	07:57:06	-196 ± 102	-454 ± 145	-257 ± 70	ndD	1657	
	2005-01-30	07:12:58	-83 ± 98	16 ± 78	-21 ± 55	nnn	1850	
NGC 2546 201	2005-01-29	06:52:31	307 ± 62	355 ± 57	594 ± 158	DDD	2650	M (new)
CPD-37 1989	2005-01-29	06:52:31	-94 ± 91	22 ± 164	-19 ± 72	nnn	2050	
HD 69004	2004-09-27	08:53:02	-100 ± 54	110 ± 116	-58 ± 48	nnn	2900	
HD 69067	2004-09-29	08:51:17	518 ± 64	554 ± 96	499 ± 52	DdD	2500	M (new)
	2004-04-20	23:29:28	609 ± 59	377 ± 78	537 ± 46	DDD	2300	M
HD 74169	2003-02-08	05:13:58	-151 ± 57	-191 ± 56	-175 ± 39	ndD	2250	m (new?)
	2004-03-02	04:38:32	-65 ± 56	-37 ± 57	-51 ± 39	nnn	2500	
HD 74535	2003-02-08	05:33:45	-83 ± 68	-126 ± 137	-96 ± 60	nnn	2250	
HD 75239	2005-01-29	08:13:02	100 ± 79	-94 ± 172	89 ± 71	nnn	2100	
HD 83002	2005-01-30	07:45:58	5 ± 80	-102 ± 161	-18 ± 70	nnn	2000	
HD 87241	2004-05-09	01:55:04	24 ± 52	-115 ± 157	26 ± 49	nnn	2800	
HD 87240	2003-02-08	07:15:26	-257 ± 58	-239 ± 103	-259 ± 50	DnD	2500	M (new)
HD 87266	2003-02-08	06:21:28	-45 ± 38	44 ± 54	0 ± 32	nnn	4100	
HD 304841	2003-02-08	06:21:28	-279 ± 78	-518 ± 163	-335 ± 69	DDD	1900	M (new)
HD 304842	2003-02-08	06:21:28	86 ± 137	-115 ± 171	-18 ± 104	nnn	2200	
HD 87405	2003-02-08	06:21:28	-82 ± 45	2 ± 65	-61 ± 36	nnn	3850	
HD 89856	2002-02-04	09:19:41	-361 ± 112	-90 ± 91	-197 ± 70	Dnd	1650	R, M (new)
HD 92190	2005-01-30	09:16:30	21 ± 79	-42 ± 149	10 ± 70	nnn	2250	
HD 92385	2005-01-29	09:28:11	-580 ± 60	-266 ± 142	-519 ± 55	DnD	2550	M (new)
Cr 228 30	2004-05-28	00:02:29	692 ± 143	405 ± 212	558 ± 113	DnD	1550	M (new)
HD 305451	2004-05-28	00:02:29	-181 ± 89	-96 ± 258	-149 ± 87	nnn	1950	
HD 96040	2005-01-29	08:48:39	-307 ± 54	-145 ± 93	-257 ± 47	DnD	2350	M (new)
HD 96729	2004-07-12	23:52:56	1125 ± 71	601 ± 100	949 ± 57	DDD	2100	M (new)
HD 303821	2005-01-30	08:35:12	-74 ± 88	-113 ± 84	-100 ± 60	nnn	1750	
HD 122983	2004-08-03	01:01:32	156 ± 54	210 ± 118	170 ± 48	dnD	3050	
HD 123183	2004-07-13	00:32:44	-440 ± 146	-181 ± 473	-409 ± 176	Dnn	1300	m (new?)
HD 123225	2004-07-13	00:32:44	97 ± 83	-176 ± 200	-22 ± 72	nnn	2400	
CPD-56 6330	2003-02-08	08:22:37	-108 ± 125	-404 ± 165	-191 ± 99	nnn	1350	
HD 127866	2003-02-08	07:52:56	-238 ± 148	-124 ± 189	-89 ± 134	nnn	1250	
CPD-57 7817	2004-07-13	02:04:24	-673 ± 69	-374 ± 130	-612 ± 60	DnD	2550	M (new)
HD 146555	2003-02-09	08:54:01	461 ± 129	232 ± 165	268 ± 97	dnn	1350	m (new?)
HD 149257	2004-07-13	02:46:41	247 ± 93	43 ± 110	160 ± 69	nnn	2350	
HD 149277	2004-07-13	02:46:41	2435 ± 149	1549 ± 186	2239 ± 104	DDD	2550	M (new)
CD-48 11051	2004-07-13	03:28:19	-2604 ± 231	-1293 ± 283	-2013 ± 117	DDD	1400	M (new)
	2004-07-24	02:51:35	-2173 ± 105	-801 ± 162	-1772 ± 74	DDD	2050	M
CD-48 11059	2004-07-13	03:28:19	217 ± 200	-15 ± 433	172 ± 173	nnn	1000	
	2004-07-24	02:51:35	193 ± 138	-145 ± 183	90 ± 107	nnn	1400	
HD 322676	2004-08-02	05:36:38	-277 ± 117	246 ± 213	-191 ± 102	nnn	2150	
HD 153948	2004-08-02	05:36:38	199 ± 58	176 ± 141	195 ± 53	DnD	3100	M (new)
NGC 6383 26	2004-08-03	04:21:50	-275 ± 217	303 ± 251	48 ± 152	nnn	1200	
HD 317857	2004-07-24	03:52:22	-1677 ± 75	-1393 ± 81	-1558 ± 54	DDD	2150	M (new)
HD 318107	2004-07-25	23:40:24	6519 ± 55	3784 ± 59	5216 ± 39	DDD	2600	9, M
HD 318100	2004-08-17	01:20:22	390 ± 71	93 ± 151	345 ± 64	DnD	2100	M (new)
CD-32 13119	2004-08-03	02:21:41	-29 ± 65	-39 ± 37	-37 ± 30	nnn	2450	
HD 318095	2004-08-03	02:21:41	101 ± 64	-168 ± 138	42 ± 54	nnn	2658	
HD 162305	2004-08-03	06:18:16	1 ± 40	122 ± 95	24 ± 37	nnn	3950	
	2004-09-26	02:18:57	112 ± 72	230 ± 150	120 ± 65	nnn	2150	
HD 320764	2004-08-23	01:44:37	-89 ± 78	-43 ± 154	-69 ± 66	nnn	2400	
HD 162725	2004-08-02	06:36:03	-67 ± 35	37 ± 115	-60 ± 33	nnn	4450	

Table A.3. continued.

ID1	Date	UT	$\langle B_z \rangle$ (G) Balmer lines	$\langle B_z \rangle$ (G) metal lines	$\langle B_z \rangle$ (G) full spectrum	Flag	SNR	Note
HD 169959	2004-07-06	03:48:34	-541 ± 58	-302 ± 128	-486 ± 52	DnD	2550	M (new)
HD 170054	2004-08-27	02:43:53	16 ± 72	361 ± 153	64 ± 68	nnn	2300	
	2004-09-23	01:21:38	254 ± 100	-207 ± 136	84 ± 77	nnn	2200	
BD-19 5044L	2004-08-23	02:34:33	-223 ± 123	-347 ± 341	-235 ± 111	nnn	1550	
BD-19 5046	2004-08-23	02:34:33	68 ± 100	64 ± 64	60 ± 92	nnn	2650	
HD 170836	2004-08-23	03:26:34	-636 ± 135	-193 ± 220	-487 ± 114	DnD	1350	M (new)
	2004-08-28	04:37:57	-633 ± 100	-449 ± 193	-583 ± 88	DdD	1950	M
	2004-09-26	02:54:12	502 ± 95	436 ± 140	483 ± 77	dDD	2100	M
HD 170860A	2004-08-04	06:40:14	-70 ± 79	62 ± 152	-41 ± 69	nnn	2050	
HD 190290	2004-07-07	08:22:31	2420 ± 110	2320 ± 48	2341 ± 41	DDD	2000	10, M

R: observed with grism 600 R.
M: definite detection according to our judgement.
(new): Star previously not known as magnetic.
m: marginal detection according to our judgement.
1: four null detections by Borra (1994; pr. comm. cited in Bychkov et al. 2003).
2: Sargent et al. (1967) reported $\langle B_z \rangle = 1300 \pm 400$ G. Several additional measurements by Conti (1970) suggest that $\langle B_z \rangle$ varies approximately from -700 to $+1400$ G.
3: Borra et al. (1983) measured $\langle B_z \rangle = 628 \pm 178$ G.
4: Field detected by Sargent et al. (1967), Conti (1970), Borra et al. (1983), Mathys & Hubrig (1997).
5: field detection reported by Bagnulo et al. (2004).
6: null detection by Bohelender et al. (1993).
7: SIMBAD coordinates are inverted (A with B and B with A). For CpD-60 944A RA and Dec are 07:56:45.3 –60:48:55; for CpD-60 944B RA and Dec are 07:56:46.3 –60:48:59.2.
8: field detection reported by Bagnulo et al. (2003).
9: Mathys & Hubrig (1997) detected $\langle B_z \rangle = 1985 \pm 230$ G.
10: Hubrig et al. (2004) detected $\langle B_z \rangle = 3220 \pm 73$ G and $\langle B_z \rangle = 3250 \pm 111$ G.

Table A.4. $\langle B_z \rangle$ measurements for stars not known to be chemically peculiar stars. Unless otherwise stated in the notes, the observations have been obtained with grism 600 B.

ID1	Date	UT	$\langle B_z \rangle$ (G) Balmer lines	$\langle B_z \rangle$ (G) metal lines	$\langle B_z \rangle$ (G) full spectrum	Flag	SNR	Note
HD 36559	2003-02-08	01:40:07	-3 ± 81	-76 ± 146	-25 ± 68	nnn	1900	
HD 36671	2003-02-08	02:08:23	69 ± 136	49 ± 70	50 ± 62	nnn	1500	
HD 37041	2003-02-08	01:11:00	125 ± 92	26 ± 70	47 ± 58	nnn	3950	
HD 37428	2003-02-08	02:49:06	-175 ± 88	-45 ± 158	-159 ± 88	nnn	2100	
HD 252214	2003-02-08	03:40:54	-49 ± 55	-11 ± 68	-26 ± 46	nnn	3350	
HD 41909	2003-02-08	03:40:54	5 ± 49	119 ± 23	104 ± 20	nDD	2900	
HD 252248	2003-02-08	03:40:54	-144 ± 108	-160 ± 104	-189 ± 77	nnn	2800	
HD 252266	2003-02-08	03:40:54	111 ± 89	-94 ± 78	-18 ± 60	nnn	2500	
NGC 2244 336	2003-02-09	03:52:60	399 ± 182	-64 ± 84	-19 ± 74	nnn	1250	
CPD-20 1637	2004-09-28	08:26:26	76 ± 67	-26 ± 194	88 ± 62	nnn	2700	
BD-20 1571	2004-09-28	08:26:26	-104 ± 81	58 ± 129	-37 ± 65	nnn	2400	
	2005-01-30	02:50:57	265 ± 108	55 ± 156	200 ± 81	dnd	1650	
NGC 2287 AR 157	2005-01-30	03:35:37	-14 ± 138	-153 ± 216	2 ± 106	nnn	1250	
CPD-20 1645	2005-01-30	03:35:37	-55 ± 88	130 ± 171	-15 ± 72	nnn	1950	
HD 52980	2005-01-30	05:03:48	-131 ± 58	-48 ± 173	-111 ± 54	nnn	2450	
BD-08 1708	2005-01-30	05:03:48	-1 ± 146	-65 ± 335	-48 ± 131	nnn	1200	
CSI-10-07049	2002-02-05	01:22:04	-234 ± 157	161 ± 134	-19 ± 76	nnn	1350	R
BD-10 1875	2002-02-05	01:22:04	-92 ± 202	-8 ± 188	-31 ± 138	nnn	1550	R
NGC 2343 22	2002-02-05	01:22:04	243 ± 218	88 ± 204	242 ± 150	nnn	1150	R
NGC 2343 40	2002-02-05	03:00:13	215 ± 238	45 ± 153	68 ± 127	nnn	750	R
CSI-10-07053 5	2002-02-05	01:22:04	320 ± 263	116 ± 253	251 ± 186	nnn	890	R
BD-10 1878	2002-02-05	03:00:13	111 ± 115	-144 ± 145	12 ± 89	nnn	1450	R
NGC 2343 25	2002-02-05	03:00:13	280 ± 246	124 ± 224	291 ± 192	nnn	1000	R
NGC 2343 16	2002-02-05	03:00:13	-225 ± 183	-162 ± 186	-227 ± 127	nnn	1350	R
BD-10 1879a	2002-02-04	03:50:42	-178 ± 228	12 ± 171	-20 ± 132	nnn	1350	R
NGC 2343 34	2002-02-04	01:35:56	-374 ± 272	169 ± 214	-40 ± 167	nnn	800	R
NGC 2343 43	2002-02-04	05:01:44	64 ± 334	34 ± 243	10 ± 181	nnn	700	R
NGC 2343 28	2002-02-05	03:00:13	164 ± 234	24 ± 181	82 ± 145	nnn	1050	R
NGC 2343 37	2002-02-04	05:01:44	-51 ± 274	21 ± 176	-59 ± 146	nnn	850	R
HD 54304	2002-02-04	02:57:20	197 ± 106	-47 ± 99	54 ± 70	nnn	2000	R
NGC 2343 27	2002-02-04	05:01:44	40 ± 262	-103 ± 212	-32 ± 164	nnn	1050	R
NGC 2343 26	2002-02-04	05:01:44	75 ± 200	-11 ± 203	32 ± 140	nnn	1200	R
NGC 2343 6	2002-02-04	02:57:20	-132 ± 107	113 ± 121	-32 ± 80	nnn	1900	R
NGC 2343 36	2002-02-04	01:35:56	-226 ± 260	388 ± 305	26 ± 193	nnn	1000	R
NGC 2343 17	2002-02-04	01:35:56	50 ± 167	-11 ± 212	-13 ± 118	nnn	1250	R
NGC 2343 10	2002-02-04	02:57:20	67 ± 113	152 ± 132	122 ± 85	nnn	1550	R
NGC 2343 31	2002-02-04	05:01:44	-71 ± 280	-530 ± 284	-296 ± 192	nnn	750	R
BD-10 1883B	2002-02-04	02:57:20	17 ± 215	70 ± 185	55 ± 139	nnn	1250	R
BD-10 1883A	2002-02-04	01:35:56	-45 ± 173	-134 ± 150	-115 ± 112	nnn	1750	R
NGC 2343 18	2002-02-04	01:35:56	76 ± 176	448 ± 214	166 ± 131	nnn	1250	R
NGC 2343 38	2002-02-04	02:57:20	187 ± 352	-123 ± 243	-23 ± 198	nnn	700	R
HD 54360	2002-02-04	01:35:56	-74 ± 166	-47 ± 102	-50 ± 85	nnn	2150	R
BD-10 1885B	2002-02-04	05:01:44	340 ± 136	-102 ± 115	89 ± 88	nnn	1750	R
HD 54388	2002-02-04	03:50:42	5 ± 64	-134 ± 54	-66 ± 41	nnn	2450	
HD 60940	2005-01-29	05:47:41	6 ± 50	97 ± 165	10 ± 47	nnn	3250	
HD 60996	2005-01-29	05:47:41	61 ± 58	93 ± 157	76 ± 57	nnn	3250	
HD 62974	2003-02-08	04:52:12	-26 ± 105	-3 ± 205	-50 ± 87	nnn	1850	
NGC 2489 59	2005-01-30	06:10:58	360 ± 169	1256 ± 372	517 ± 181	ndn	1300	
HD 65691	2002-02-05	06:03:02	-158 ± 215	-344 ± 172	-262 ± 134	nnn	1500	R
CPD-60 942	2002-02-05	06:03:02	616 ± 281	-208 ± 216	106 ± 169	nnn	950	R
CD-60 1929	2002-02-05	06:03:02	-52 ± 109	244 ± 108	110 ± 76	nnn	2100	R
CD-60 1932	2002-02-05	06:55:01	-110 ± 338	-144 ± 231	-99 ± 188	nnn	1100	R
	2002-02-05	06:03:02	-28 ± 305	7 ± 225	-35 ± 178	nnn	1200	R
HD 65869	2002-02-05	06:55:01	233 ± 118	-203 ± 107	-5 ± 79	nnn	2750	R
HD 65896	2002-02-04	07:54:30	109 ± 111	144 ± 98	127 ± 73	nnn	1900	R
HD 65950	2002-02-05	07:45:43	-32 ± 50	-123 ± 62	-114 ± 50	nnn	2800	R
V373 Car	2004-03-08	05:25:21	-187 ± 75	-34 ± 61	-104 ± 48	nnn	1350	

Table A.4. continued.

ID1	Date	UT	$\langle B_z \rangle$ (G) Balmer lines	$\langle B_z \rangle$ (G) metal lines	$\langle B_z \rangle$ (G) full spectrum	Flag	SNR	Note
	2002-02-05	04:19:29	-87 ± 23	-25 ± 36	-66 ± 19	DnD	1600	R
HD 65949	2002-02-04	07:54:30	-19 ± 89	158 ± 83	74 ± 61	nnn	2250	R
BD-60 969	2002-02-04	07:54:30	43 ± 136	-138 ± 107	-69 ± 84	nnd	2350	R
BD-60 975	2002-02-05	04:19:29	145 ± 111	100 ± 111	127 ± 78	nnd	2250	R
	2002-02-04	06:08:09	65 ± 123	229 ± 140	132 ± 89	nnn	2250	R
CPD-60 977	2002-02-04	07:01:42	35 ± 109	75 ± 94	57 ± 70	nnn	1550	R
V410 Car	2002-02-04	07:01:42	77 ± 225	-200 ± 188	-98 ± 140	nnn	1450	R
V392 Car	2004-03-08	05:25:21	221 ± 129	-75 ± 144	111 ± 91	nnn	1250	
	2002-02-05	04:19:29	-4 ± 97	85 ± 73	34 ± 57	nnn	2000	R
	2002-02-05	07:45:43	-285 ± 220	82 ± 142	15 ± 119	nnn	1200	R
CD-60 1967	2002-02-04	06:08:09	20 ± 32	49 ± 59	32 ± 28	nnn	2700	R
CD-60 1971	2002-02-04	06:08:09	252 ± 149	46 ± 96	101 ± 80	nnn	2600	R
V417 Car	2002-02-04	07:54:30	-78 ± 130	-175 ± 112	-73 ± 80	nnn	1400	R
CPD-60 984	2002-02-04	07:01:42	33 ± 137	170 ± 103	52 ± 77	nnn	1500	R
CPD-60 986	2002-02-04	07:01:42	-62 ± 160	-47 ± 153	-38 ± 109	nnn	1825	R
V418 Car	2002-02-05	04:19:29	-9 ± 222	98 ± 172	68 ± 133	nnn	1190	R
CD-60 1974	2002-02-05	04:19:29	-301 ± 154	-24 ± 119	-126 ± 94	nnn	2100	R
	2004-03-08	05:25:21	-168 ± 128	139 ± 360	-165 ± 121	dnd	1350	
CD-60 1975	2002-02-04	06:08:09	0 ± 122	-116 ± 100	-48 ± 76	nnn	2100	R
CD-60 1976	2002-02-04	07:01:42	-50 ± 182	-12 ± 121	-58 ± 104	nnn	1850	R
CD-60 1979	2002-02-05	07:45:43	-210 ± 269	-109 ± 276	-162 ± 191	nnn	1050	R
CD-60 1978	2002-02-04	07:01:42	145 ± 216	96 ± 244	67 ± 161	nnn	1300	R
CD-60 1981	2002-02-05	07:45:43	414 ± 220	-77 ± 161	167 ± 141	nnn	1000	R
V420 Car	2002-02-05	04:19:29	-29 ± 215	-227 ± 172	-127 ± 134	nnn	1500	R
HD 66137	2002-02-04	07:01:42	-124 ± 160	110 ± 125	53 ± 100	nnn	1800	R
HD 66194	2002-02-04	06:08:09	-183 ± 97	-237 ± 353	-197 ± 93	nnn	600	R
CD-60 1996	2002-02-05	05:08:50	457 ± 207	744 ± 206	631 ± 159	nDD	1000	R
	2003-02-09	06:30:09	81 ± 169	98 ± 147	108 ± 120	nnn	1200	
CD-60 1999	2003-02-09	06:30:09	100 ± 289	-67 ± 91	-53 ± 87	nnn	1050	
	2002-02-05	05:08:50	80 ± 233	-289 ± 205	-83 ± 149	nnn	1350	R
[N75] 195	2005-01-30	07:12:58	68 ± 103	-25 ± 79	34 ± 58	nnn	2300	
[N75] 196	2004-09-27	07:57:06	183 ± 166	444 ± 386	603 ± 144	nnd	1400	
	2005-01-30	07:12:58	-40 ± 162	-170 ± 202	-50 ± 127	nnn	1450	
NGC 2546 272	2004-09-27	07:57:06	26 ± 96	61 ± 207	22 ± 86	nnn	2350	
	2005-01-30	07:12:58	188 ± 126	-21 ± 125	24 ± 97	nnn	2000	
CD-37 4353	2005-01-29	06:52:31	-126 ± 71	-30 ± 346	-102 ± 69	nnn	2450	
HD 69003	2004-09-27	08:53:02	-48 ± 53	-151 ± 259	-42 ± 51	nnn	3500	
HD 298537	2005-01-30	07:45:58	-221 ± 334	-402 ± 238	-293 ± 178	nnn	750	
HD 298536	2005-01-30	07:45:58	49 ± 196	-105 ± 508	-86 ± 179	nnn	950	
NGC 3114 233	2003-02-08	07:15:26	-123 ± 96	53 ± 191	-87 ± 85	nnn	1850	
CPD-59 1698	2003-02-08	06:21:28	1 ± 126	-333 ± 406	-9 ± 115	nnn	1650	
CPD-59 1700	2003-02-08	07:15:26	287 ± 161	32 ± 240	212 ± 133	nnn	1400	
CPD-59 1703	2003-02-08	06:21:28	-106 ± 118	-165 ± 219	-128 ± 98	nnn	1550	
HD 298051	2002-02-04	09:19:41	-395 ± 213	-61 ± 245	-250 ± 160	nnn	1150	R
HD 89901	2002-02-05	08:36:32	-153 ± 163	250 ± 156	39 ± 113	nnn	2050	R
HD 89900	2002-02-05	08:36:32	-3 ± 136	-1 ± 135	0 ± 96	nnn	2050	R
HD 89915	2002-02-05	08:36:32	37 ± 176	-189 ± 121	-113 ± 100	nnn	2600	R
HD 89922	2002-02-04	09:19:41	-47 ± 130	-23 ± 112	-46 ± 84	nnn	1800	R
HD 298047	2002-02-05	08:36:32	1 ± 179	154 ± 233	94 ± 143	nnn	1550	R
HD 89938	2002-02-05	08:36:32	-152 ± 181	-10 ± 206	-91 ± 136	nnn	1600	R
HD 89937	2002-02-05	08:36:32	14 ± 190	120 ± 154	71 ± 120	nnn	1600	R
HD 89956	2002-02-05	09:20:10	-374 ± 337	20 ± 222	-81 ± 185	nnn	1350	R
CPD-51 3249	2003-02-09	08:13:16	-54 ± 200	-16 ± 173	-51 ± 138	nnn	1300	
HD 298053	2003-02-09	08:13:16	60 ± 98	105 ± 111	116 ± 84	nnn	1700	
HD 303107	2005-01-30	09:16:30	-253 ± 143	915 ± 430	-190 ± 133	nnn	1350	
HD 305535	2004-05-28	00:02:29	-26 ± 64	225 ± 123	30 ± 55	nnn	3000	
HD 305543	2004-05-28	00:02:29	-4 ± 224	-149 ± 121	-105 ± 90	nnn	2700	
HD 96653	2004-07-12	23:52:56	87 ± 45	824 ± 486	96 ± 44	nnn	1600	
NGC 3532 447	2004-07-12	23:52:56	-70 ± 101	456 ± 324	-3 ± 95	nnn	2000	

Table A.4. continued.

ID1	Date	UT	$\langle B_z \rangle$ (G) Balmer lines	$\langle B_z \rangle$ (G) metal lines	$\langle B_z \rangle$ (G) full spectrum	Flag	SNR	Note
HD 96790	2004-07-12	23:52:56	-168 ± 174	-118 ± 126	-159 ± 98	nnn	2150	
CD-47 8868	2004-08-03	01:01:32	3 ± 89	-284 ± 290	-16 ± 84	nnn	2000	
HD 123201B	2004-07-13	00:32:44	-109 ± 96	353 ± 281	-77 ± 94	nnn	1700	
HD 127835	2003-02-08	09:03:56	87 ± 85	-5 ± 184	77 ± 78	nnn	2050	
CPD-56 6334	2003-02-08	08:22:37	80 ± 140	-191 ± 158	-33 ± 92	nnn	1950	
NGC 5662 126	2003-02-08	08:22:37	233 ± 141	104 ± 172	187 ± 109	nnn	1450	
HD 127900	2003-02-08	09:03:56	-7 ± 56	236 ± 126	30 ± 52	nnn	2700	
HD 127924	2003-02-08	09:03:56	20 ± 100	-22 ± 125	25 ± 88	nnn	2050	
NGC 6087 129	2004-07-13	02:04:24	-5 ± 69	133 ± 175	46 ± 62	nnn	2750	
TYC 8719- 717-1	2004-07-13	02:04:24	0 ± 84	266 ± 171	51 ± 74	ndn	2300	
HD 146484	2003-02-09	08:54:01	-247 ± 100	-316 ± 258	-222 ± 98	nnd	1600	
CD-48 11050	2004-07-13	03:28:19	-148 ± 114	129 ± 325	-47 ± 98	nnn	1550	
	2004-07-24	02:51:35	-55 ± 74	26 ± 187	-11 ± 63	nnn	2200	
CD-48 11060	2004-07-13	03:28:19	-143 ± 172	59 ± 310	-102 ± 136	nnn	1250	
	2004-07-24	02:51:35	-99 ± 112	-228 ± 161	-95 ± 87	nnn	1850	
HD 323673	2004-08-02	05:36:38	-43 ± 91	97 ± 210	1 ± 81	nnn	2150	
NGC 6383 28	2004-08-03	04:21:50	134 ± 145	-30 ± 448	17 ± 143	nnn	1250	
NGC 6383 700	2004-08-03	04:21:50	177 ± 186	62 ± 187	148 ± 116	nnn	1250	
NGC 6383 87	2004-08-03	04:21:50	78 ± 137	68 ± 175	35 ± 106	nnn	1250	
HD 317846	2004-07-24	03:52:22	-20 ± 74	-77 ± 193	-23 ± 68	nnn	2700	
NGC 6383 102	2004-07-24	03:52:22	163 ± 109	-221 ± 327	147 ± 101	nnn	1750	
HD 317852	2004-08-03	04:21:50	-61 ± 131	34 ± 71	-28 ± 65	nnn	1700	
HD 318108	2004-07-25	23:40:24	-131 ± 79	-156 ± 350	-98 ± 82	nnn	2150	
HD 318109	2004-07-25	23:40:24	67 ± 87	62 ± 442	93 ± 90	nnn	1950	
CD-32 13089	2004-08-17	01:20:22	-19 ± 94	76 ± 126	57 ± 68	nnn	2000	
CD-32 13093	2004-08-17	01:20:22	-156 ± 113	-406 ± 344	-245 ± 106	nnn	1700	
V976 Sco	2004-08-17	01:20:22	-62 ± 214	-199 ± 279	-84 ± 142	nnn	950	
HD 318099	2004-08-17	01:20:22	-40 ± 84	587 ± 363	-38 ± 89	nnn	1850	
HD 320765	2004-08-23	01:44:37	-18 ± 71	281 ± 235	0 ± 65	nnn	2500	
HD 162678	2004-08-02	06:36:03	-2 ± 36	-14 ± 132	3 ± 34	nnn	4150	
HD 162724	2004-08-02	06:36:03	-33 ± 54	-329 ± 171	-53 ± 51	nnn	5200	
BD-19 5044 F	2004-08-23	02:34:33	94 ± 100	-2 ± 255	63 ± 96	nnn	2050	
BD-19 5045 ?	2004-08-23	02:34:33	-12 ± 74	191 ± 120	86 ± 60	nnn	2650	
BD-19 5044 M	2004-08-23	02:34:33	-50 ± 127	244 ± 492	-32 ± 120	nnn	1450	
HD 170835	2004-08-23	03:26:34	-242 ± 239	-500 ± 310	-417 ± 183	nnn	1500	
	2004-08-28	04:37:57	-15 ± 200	-635 ± 235	-435 ± 142	nnD	2100	

Table A.5. $\langle B_z \rangle$ measurements for stars not of early spectral type.

ID1	ID2	V	Spectral type	Date	UT	$\langle B_z \rangle$ (G) full spectrum	Flag	SNR	Note
NGC 2244 330	NGC 2244 PS 537	10.8	K5	2003-02-09	03:52:60	90 ± 18	d	2300	
NGC 2244 365	GSC 00154-00486	11.9	G2	2003-02-09	03:52:60	0 ± 51	n	1600	
NGC 2244 364	GSC 00154-00074	12.2	–	2003-02-09	03:52:60	53 ± 35	n	1200	
NGC 2287 AR 155	–	–	–	2005-01-30	03:35:37	-32 ± 103	n	1300	
NGC 2343 15	CSI-10-07056 2	11.4	[K4?]	2002-02-04	01:35:56	28 ± 35	n	1550	R
NGC 2343 23	CSI-10-07057 5	11.9	[F2?V]	2002-02-04	02:57:20	-55 ± 66	n	1050	R
NGC 2343 19	CSI-10-07058 2	11.5	[G/K?]	2002-02-04	01:35:56	-220 ± 121	n	1350	R
HD 54387	BD-10 1885	8.5	G5	2002-02-04	01:35:56	69 ± 26	n	1500	R
HD 60968	BD-14 2017	9.2	K0	2005-01-29	05:47:41	-47 ± 25	n	2600	
NGC 2516 DAC 515	NGC 2516 SBL 481	11.3	–	2002-02-05	07:45:43	167 ± 166	n	750	R
CD-60 1997	NGC 2516 SBL 953	10.4	[F2/3?V]	2002-02-05	05:08:50	74 ± 48	n	1150	R
				2003-02-09	06:30:09	107 ± 37	d	1450	
HD 298045	CD-51 4704	9.4	M3	2003-02-09	08:13:16	190 ± 32	D	1750	
HD 298054	CD-51 4707	9.8	G0	2003-02-09	08:13:16	29 ± 16	n	1750	
CPD-58 3151	NGC 3532 198	10.0	[G0/2]	2004-07-12	23:52:56	-27 ± 59	n	1800	
CD-47 8861	NGC 5460 38	9.8	–	2004-08-03	01:01:32	-59 ± 34	n	2100	
NGC 5460 73	CD-47 8891	9.6	K5	2004-07-13	00:32:44	55 ± 48	n	1400	
HD 127753	CD-55 5722	7.1	K5III	2003-02-08	07:52:56	44 ± 15	n	1650	
NGC 5662 118	CSI-56-14321 1	10.7	[K5V]	2003-02-08	08:22:37	-22 ± 35	n	1200	
NGC 5662 CLB 149	GSC 08687-01270	11.5	[?]	2003-02-08	09:03:56	153 ± 61	n	550	
CPD-57 7883	PPM 772347	9.6	–	2003-02-09	08:54:01	69 ± 87	n	1100	
CD-34 11864	NGC 6396 PPM 78	10.6	M4	2003-02-09	09:27:31	96 ± 39	n	700	
NGC 6405 322	–	–	–	2004-08-03	02:21:41	64 ± 49	n	2000	